Published in final edited form as:

Cancer Res. 2017 September 15; 77(18): 5077–5094. doi:10.1158/0008-5472.CAN-17-0829.

TBK1 Provides Context-Selective Support of the Activated AKT/mTOR Pathway in Lung Cancer

Jonathan M. Cooper[1], **Yi-Hung Ou**[1,2], **Elizabeth A. McMillan**[1], **Rachel M. Vaden**[1], **Aubhishek Zaman**[1], **Brian O. Bodemann**[1], **Gurbani Makkar**[1], **Bruce A. Posner**[3], and **Michael A. White**[1,*]

[1]Department of Cell Biology, UT Southwestern Medical Center, Dallas, TX 75390, USA

[3]Department of Biochemistry, UT Southwestern Medical Center, Dallas, TX 75390, USA

Abstract

Emerging observations link dysregulation of TANK-binding kinase 1 (TBK1) to developmental disorders, inflammatory disease, and cancer. Biochemical mechanisms accounting for direct participation of TBK1 in host defense signaling have been well described. However, the molecular underpinnings of the selective participation of TBK1 in a myriad of additional cell biological systems in normal and pathophysiological contexts remain poorly understood. To elucidate the context-selective role of TBK1 in cancer cell survival, we employed a combination of broad-scale chemogenomic and interactome discovery strategies to generate data-driven mechanism-of-action hypotheses. This approach uncovered evidence that TBK1 supports AKT/mTORC1 pathway activation and function through direct modulation of multiple pathway components acting both upstream and downstream of the mTOR kinase itself. Furthermore, we identified distinct molecular features in which mesenchymal, Ras-mutant lung cancer is acutely dependent on TBK1-mediated support of AKT/mTORC1 pathway activation for survival.

Keywords

TBK1; mTOR/AKT; KRAS; Mesenchymal; NSCLC

Introduction

Oncogenic Ras mutations are found in approximately 30% of all human cancers. The likely causal participation of these mutations in the mechanistic etiology of neoplastic disease has provoked extensive efforts to directly and/or indirectly intercept oncogenic Ras activity for therapeutic benefit (1). Within the Ras effector network, signaling through RalA/B GTPase/exocyst complexes has been directly implicated in Ras-mediated tumorigenic transformation (2,3). This is mediated at least in part by activation of the serine/threonine protein kinase TANK-binding kinase 1 (TBK1) (4–6). However, the key mechanistic contributions of

*Correspondence to: Michael A. White, Ph.D., Department of Cell Biology, UT Southwestern Medical Center, Dallas, TX 75390-9039, Phone: 214-648-4212; Fax: 214-648-5814; Michael.White@utsouthwestern.edu.

[2]Current address: Department of Pharmacology, Weill Cornell Medical College, New York, NY 10065, USA

Conflicts of Interest Disclosure:

Michael A. White is currently Chief Scientific Officer and Vice President of Tumor Cell Biology at Pfizer, Inc. The authors declare no other potential conflicts of interest.

TBK1 to cancer cell biology and the selective settings where these contributions are most manifest, is poorly understood.

TBK1 is an atypical IkB kinase that, together with its homologue, IKKe, mediates classic innate immunity by inducing type 1 interferon gene expression in response to pathogen exposure through direct activation of IRF3/7 (7,8). However, TBK1 kinase activity also supports additional cell biological systems, through distinct substrate proteins, that regulate cell growth, self-renewal, pathogen clearance, and organellar function (5,6,9,10). Pathological perturbation of TBK1 regulation has been linked to neoplastic, autoimmune and neurodegenerative diseases in mice and humans (11–13).

To help parse TBK1 mechanism/disease relationships, we initiated data-driven studies to deconvolve the context-selective role of TBK1 in cancer cell survival. High-throughput chemogenomic profiling of TBK1 inhibitors in parallel with broad-scale TBK1 interactome characterization, and validation within the context of pro-growth signaling, was used to deliver evidence-based hypotheses for TBK1 support of tumorigenicity. Collectively, this investigation revealed a distinct biological context, specified by collaborative activity of mutant Ras and mesenchymal cell fate regulatory programs, in which TBK1 supports mTORC1 pathway activation to promote cell survival.

Materials and Methods

Cell Culture

All HEK293T, HEK293FT, MNT1, HCT116, HeLa, and Mouse Embryonic Fibroblasts (MEFs) cell lines were cultured in Dulbecco's Modified Eagle Medium (DMEM), containing 10% Fetal Bovine Serum (FBS) (Atlanta Biologicals) and 1% antibiotics (Penicillin/Streptomycin, Life-Technologies (15140-163) or Invitrogen (15140122)). MNT1 cells were generously provided by Dr. Michael Marks (University of Pennsylvania) circa 2006. HEK293FT cells were kind gifts from Dr. William Hahn (Dana-Farber Cancer Institute) in 2007. HEK293T and HeLa cells were obtained from ATCC circa 2007–2008. Non-Small Cell Lung Cancer (NSCLC) lines (A549, HCC44, A427, HCC4017, H1573, H2347, and H2887) were obtained originally from Drs. John Minna and Adi Gazdar (UTSW) circa 2004 and were cultured in Roswell Park Memorial Institute (*RPMI*) 1640 Medium, containing 5% FBS and 1% antibiotics. Authentication for NSCLC and melanoma (MNT1) cell lines was conducted by the McDermott Center Sequencing Core at UTSW (Promega PowerPlex® Fusion System). *Tbk1* homozygous Wild-Type (WT) and homozygous knock-out (−/−) MEFs were derived as reported in (6). *Tbk1* kinase domain homozygous Wild-Type (+/+), heterozygous mutant (+/Δ), and homozygous mutant (Δ/Δ) MEFs were generated in our laboratory in 2012 by a modified 3T9 protocol (14) (regularly serially passaged until cells exited quiescent state [approx. 2–3 months]) from mice described in (15), generously provided by Dr. Rolf Brekken (UTSW). *Trp53−/−* immortalized *Tsc2* WT and *Tsc2* −/− MEFs were generously provided by Dr. James Brugarolas (UTSW) in 2012. HCT116 *PDPK1* WT and *PDPK1* homozygous knock-out (−/−) cells were kind gifts from Dr. Bert Vogelstein (Johns Hopkins University) in 2010. HCC44 LKB1-overexpressing cells were generated in our laboratory by Dr. JiMi Kim (UTSW) in 2013. Authentication for knockout and overexpression cell lines was conducted

by Western Blotting. Routine mycoplasma testing of the cell lines was not performed. Recorded cell line source and timeframe of acquisition information is as noted above.

Antibodies and Other Materials

The following antibodies were from Cell Signaling Technologies (CST): anti-4E-BP1-pT37/46, 2855; anti-ACC, 3662, 3676; anti-ACC-pS79, 3661; anti-AKT1, 2938, 2967; anti AKT (pan), 4691; anti-AKT-pT308, 4056; anti-AKT-pS473, 4060; anti-Claudin-1, 13255; anti-E-Cadherin, 3195; anti-ERK1/2, 4695, anti-GAPDH, 5174; anti-LKB1, 3047; anti-LKB1-pS428, 3051; anti-mTOR, 2983; anti-mTOR-pS2448, 2971; anti-mTOR-pS2481, 2974; anti-PRAS40, 2691; anti-PRAS40-pT246, 2997; anti-Raptor, 2280; anti-S6, 2217; anti-S6-pS235/236, 4858; anti-S6K, 2708, 9202; anti-S6K-pT389, 9234; anti-S6K-pT421/pS424, 9204; anti-SMAD2-pS465/467, 3108; anti-Snail, 3879; anti-TBK1, 3504; anti-TBK1-pS172, 5483; anti-TSC2, 3635; anti-ULK1, 4773; anti-Vimentin, 5741; anti-ZEB1, 3396). The rabbit anti-IKKe antibody (Z5020108) was from BioChain. The mouse anti-E-Cadherin (36/E-Cadherin) monoclonal antibody (610181) was from BD Biosciences. The mouse anti-Sec5 antibody was generously provided by Dr. Charles Yeaman (University of Iowa). The mouse anti-Exo70 antibody was generously provided by Dr. Shu-Chan Hsu (Rutgers University). MEM Essential Amino Acid Solution (EAA) (M5550), Mouse anti-beta-tubulin (2-28-33) monoclonal antibody (T5193), Rabbit anti FLAG (SIG1-25) monoclonal antibody (F2555), mouse anti-FLAG monoclonal antibody (M2) (F1804), and anti-FLAG monoclonal antibody (M2)-conjugated beads (A2220) were from Sigma-Aldrich. Protein A/G beads (sc-2003), rabbit anti-c-Myc (A-14) polyclonal antibody (sc-789), rabbit anti-ERK1/2 (C16) polyclonal antibody (sc-93), rabbit anti-HA (Y-11) polyclonal antibody (sc-805), mouse anti-HA (F-7) monoclonal antibody (sc-7392), and anti-HA antibody conjugated beads (sc-7392ac) were from Santa Cruz Biotechnology. cOmplete, Mini, EDTA-free Protease Inhibitor Cocktail Tablets (04693159001) were from Roche. 5X Protein Reagent was from Cytoskeleton Inc. (ADV01-A). Pre-cast polyacrylamide gels (4–15%, 4561086; 4–20%, 456-4093) were from Bio-Rad. RNAiMax was from Invitrogen (13778-150). BCA Protein Quantification Kit (23225), MK-2206 (508726), Peirce Enhanced chemiluminescence substrate (ECL) (32106), SuperSignal West-Pico ECL, (34080), and SuperSignal West-Femto ECL (PI-34096) were from Thermo Fischer Scientific. Torin 1 was from Tocris (4247). Rapamycin was from LC Laboratories (R-5000). cDNA transfection reagent Fugene 6 (E2691), Cell Titer Glo (G7573), and Caspase-Glo (G8091/2/3 series) were from Promega. Recombinant S6K (H00006198-P01) was from Abnova. Lambda Protein Phosphatase (P0753S) was from New England BioLabs (NEB). Recombinant active TBK1 (14-628) and BX795 (204001) were from EMD Millipore. Rag and LKB1 plasmids were from Addgene (pRK5-HA GST RagA WT, 19298; pRK5-HA GST RagB WT, 19301; pRK5-HA GST RagC WT, 19304; pRK5-HA GST RagD WT, 19307; pRK5-HA GST RagD 77L, 19308; pRK5-HA GST RagD 121L, 19309; pBabe-FLAG-LKB1-WT, 8592; pBabe-FLAG-LKB1-KD (K78I), 8593). GSK2292978A was generously provided by Dr. Seng-Lai "Thomas" Tan (Amgen). The HA-TBK1 plasmid was generously provided by Dr. Xuetao Cao (Second Military Medical University, Shanghai, China). The HA-S6K plasmid was generously provided by Dr. Kun-Liang Guan (University of California, San Diego). Source of the 6-amino pyrozolopyrimidine Compound II and TBK1 plasmids (pRK5-myc-FLAG-TBK1-WT, pR5K-myc-FLAG-TBK1-K38M (KD) was (5).

TBK1 Compound Screen/Cell Viability Dose-Response Curve (DRC)

TBK1 inhibitors BX795 and Compound II were tested among 100 NSCLC cell lines by the UTSW High-Throughput Screening (HTS) Core Facility. Briefly, cells were plated in 384-well cell culture plates and subsequently treated for 96 hrs in the presence of DMSO or compound in 12-point, half-log doses ranging from 50μM to 50pm. Cell viability was assayed post-treatment via Cell-Titer Glo (Promega). Chemical response for each cell line was converted to an activity score with the following equation:

$$\mathrm{AC} = -1 * (100 - \frac{x}{\mathrm{median}(x_{\mathrm{control}})} * 100)$$

so that an activity score indicates percent kill relative to on-board controls. We found normalizing to the median of the two lowest doses, as opposed to on-board DMSO controls, in the final dataset minimized plate effects and resulted in a better curve fit and a more accurate description of sensitivity. We used the drc package in R to fit a standard 4 parameter log-logistic fit to the data and discover ED50 values. As imputed ED50 values have shown to be problematic in re-tests of large drug screening datasets, we do not impute values. Rather, if the imputed ED50 value would be greater than the top tested dose (50μM), we assign an ED50 of the top dose. Additionally, to correct for low ED50 values being assigned to chemicals in which the response is shallow, we assign an ED50 value of the top tested dose if the chemical does not result in at least 30% reduction in CTG values.

We calculated AUC values by determining area under the curve of the log fitted hill equation through standard integral analysis. For many of the compounds, a large population of the dose range is completely innocuous for all cell lines tested. To increase the dynamic range with AUC values, we found for each compound the proportion of the curve in which there is a response across all cell lines, and eliminated the data for the lower doses. Each compound was tested in 2 separate runs, with three replicates per run. To automatically detect the best, most reproducible data, we select the two replicates from each run with the best concordance between calculated ED50 values. The reported ED50 or AUC values are the mean between the filtered runs. See Table S1 for full DRC results.

Compound-Compound Correlations

For correlations comparing BX795 and Compound II to each other or to cell growth rates, correlation plots, linear regression best-fit lines, and statistics were generated using GraphPad Prism. Correlations in overlapping sets of NSCLC lines were calculated for Log_{10}-transformed BX795 or Compound II ED50 values vs. published inhibitor values (ln IC50 (16) or Area-Under-the-Curve (AUC) (Log_{10}-transformed) (17)). Correlation plots, linear regression best-fit lines, and statistics for these analyses were generated using R. Pearson values represent the correlation for a given compound pair among either all (r(all)) or *KRAS*-mutant only (r(mut)) NSCLC lines per analysis. See Table S2 for full analysis results.

Essential Amino Acid (EAA) Nutrient Stimulation

Cells were plated in 35mm or 6-well cell culture dishes in 2mL of cell culture media. The next day, cell culture media was aspirated and 2mL of 1X Earle's Balanced Salt Solution (EBSS) was added for 3 hrs. During the final hour of EBSS treatment, cells were “primed” by the addition of L-glutamine (Gln) in EBSS to a final concentration per well of 1mM or 2mM. MEM-Essential Amino Acids Solution (EAA) (Sigma Aldrich) was added to a final concentration per well of 1X for the times listed. All media were then aspirated, cells were washed once in cold 1X PBS (usually supplemented with phosphatase inhibitors NaF, β-glycerophosphate and sodium orthovanadate) and then lysed either in NP-40 buffer (50mM Tris HCl, 120mM NaCl, 0.5% NP40, 1mM EDTA, 1mM DTT), plus phosphatase inhibitors (NaF, β-glycerophosphate and sodium orthovanadate) and protease inhibitors tablet (Roche cOmplete Mini) or in 2% SDS buffer (50mM Tris pH 6.8, 2% SDS, 10% glycerol). Following lysis on ice at 4C, SDS lysates were heated at ≥ 95C for ≥ 5 min and then protein concentration was measured via Pierce BCA assay. Protein concentration was equilibrated across experimental samples and Western Blot samples were prepared using 2X Sample Buffer (+β-me) and heated to ≥ 95C for ≥ 5 min. NP40 lysates were lysed for 15 min at 4C and then centrifuged at 20,000g for 20 min at 4C, and the protein concentration of the supernatant was quantified using Advanced Protein Assay Reagent (Cytoskeleton, modified Method 4). Protein concentration was equilibrated across experimental samples and Western Blot samples were prepared using 6X Sample buffer (+β-me) and heated to ≥ 95C for ≥ 5 min.

SDS-PAGE and Immunoblotting

Equivalent amounts (μg) of Western Blot lysates were loaded and run in multiple self-poured (6%, 8%, or 10%) or pre-cast (4%–20% or 4%–15% gradients, from Bio-Rad) polyacrylamide gels. Gels were transferred to Polyvinylidene difluoride (PVDF) membranes using standard wet-tank transfer or Bio-Rad TransBlot Turbo Semi-Dry transfer protocols. Membranes were blocked in 5% non-fat milk/Tris-buffered saline w/Tween (TBST) for 1 hr. Primary antibodies were diluted in TBST, 5% non-fat milk/TBST, or 5% Bovine Serum Albumin (BSA)/TBST, each w/ 0.05% Sodium Azide, and incubated overnight at 4C. Primary antibody dilutions were saved for reuse and membranes were washed with TBST before HRP-linked secondary antibodies were added in 5% non-fat milk/TBST at Room Temperature (RT) for 1 hr. Pierce enhanced chemiluminescence (ECL) was added and Horseradish Peroxidase (HRP)-catalyzed luminescence was captured on autoradiography film.

TBK1 adaptor-focused screen

HeLa cells were transfected via RNAiMax (Invitrogen) for 72 hrs with siRNA pools consisting of three independent oligonucleotide duplexes (Sigma) against the listed gene targets. Transfections were conducted in batches, in which 2 or 3 members of the TBK1 interactor network were knocked down alongside a *LONRF1* negative control siRNA pool. Transfections were conducted approximately 16–18 hrs after plating cells. The day after the transfection, the transfection media was replaced with fresh culture media. Three days post-transfection the cells were washed with EBSS once and then incubated with EBSS for 3 hrs

(including priming with 2mM L-Gln in EBSS for the final hour). The cells were then stimulated with 1X EAA for the indicated time points. Samples within each transfection batch were analyzed together by SDS-PAGE, followed by immunoblot for total Ribosomal S6 and phospho-S6 (pS235/236). Relative phospho-S6/total S6 densitometry ratios for each knockdown were calculated via ImageJ and normalized relative to the *LONRF1* + 30 min EAA condition within each batch. Error bars = standard deviation from the mean. Two-tailed unpaired Student's t tests were performed between *LONRF1* + 10 min EAA or *LONRF1* + 30 min EAA and the respective time points of the other siRNA pools within each batch. *P < 0.05, **P < 0.01, ***P < 0.001, ****P < 0.0001.

TBK1 IP-Mass-Spec

Cloning—Wild-type (WT) TBK1 was PCR amplified from a FLAG-TBK1 vector using primers with an overhang 5' NOT1 and a 3' KPN1 site and cloned into an N-terminal 3XFLAG pIRESpuro (Invitrogen) vector by dual restriction digestion of vector and insert with the aforementioned enzymes followed by ligation with T4 DNA ligase.

Immunoprecipitation—$3X10^6$ HEK293T cells were seeded in four 10 cm dishes per condition in 10 ml DMEM-10% FBS. Next day, cells were transfected with either 3μg of 3XFlag-TBK1 plasmid or 3XFlag-Empty Vector (control) using Fugene 6 (Promega) at a ratio of 3:1 (μL Fugene 6 to μg DNA). 48 hrs post-transfection, the cells were lysed in immunoprecipitation lysis buffer (20 mM Tris-HCl pH 7.4, 137mM NaCl, 1% Triton X-100, 0.5% sodium deoxycholate, 10mM MgCl2, 2mM EGTA) plus protease and phosphatase inhibitors (Roche EDTA-free cOmplete ULTRA and PhosphoSTOP). Cells were lysed for 1 hr and cleared at 16,000g for 10 min at 4C. 1500mg of lysate was brought to a concentration of 1.5mg/mL by dilution with lysis buffer, and the immunoprecipitation was carried out for 14 hrs at 4C using 2.5μg of monoclonal anti-Flag M2 (Sigma) or mouse monoclonal anti-HA F-7 (Santa Cruz) antibodies. Antibody-antigen complexes were isolated by the addition 90μl of Protein A/G-agarose beads (Santa Cruz) for 2 hrs at 4C. Complexes were then washed in lysis buffer 4 times for 1 min at 4C and finally eluted with 90μl 2X SDS sample buffer (BioRad, 161-0737) followed by heating at ≥ 95C for 12 min. IP samples were then run on a precast SDS-PAGE 4–20% gradient gel (Bio-Rad) and run until the dye front was approximately 15mm into the gel. The gel was washed with dH_20 and stained with colloidal Coomassie for 1 hr at RT to visualize and fix, followed by another 30 min dH_20 wash. For each sample, fixed immunoprecipitated proteins separated on the gel were excised as a single fragment with sterile scalpel and homogenized in an Eppendorf tube with a sterile needle. The samples were submitted for mass spectrometry using Orbitrap Fusion Lumos™ by the UTSW Proteomics core.

MS/MS Data analysis—LC-MS/MS data was generated and quantified using spectral count-based, semi-quantitative label-free quantification (18). The finalized dataset was further controlled for false positives using the "CRAPOME" database (www.crapome.org.) to exclude commonly identified non-specific interactors. High stringency inclusion criteria cutoffs allowed proteins to pass if they were identified in less than 5% of the reports within the CRAPOME database, absent in the 'tag-only' IP condition, and present in FLAG-

specific pull down with at least 2 spectral counts. This identified TBK1 (the top hit), Raptor (*RPTOR*), and S6K (*RPS6KB1*) among the top 12 TBK1-specific hits.

Immunoprecipitations (IPs)

IPs in HEK293T cells were conducted as in (5). Briefly, whole cell extracts were prepared by lysing cells in IP lysis buffer (20 mM Tris HCl [pH 7.5], 10 mM MgCl2, 2 mM EGTA, 10% Glycerol, 137 mM NaCl, 1% Triton X-100, 0.5% Na Deoxycholate, 1 mM DTT) plus phosphatase and protease inhibitors (Roche). Lysates were incubated with anti-TBK1 rabbit monoclonal antibody (Cell Signaling, Cat #3504) and 30μL Protein A/G beads (Santa Cruz) overnight at 4C. Immunoprecipitates were washed three times in IP lysis buffer plus 1 mM PMSF then heated to ≥ 95C for ≥ 5 min in standard SDS sample buffer. Samples were separated by SDS-PAGE followed by Western blot analysis. IP of overexpressed proteins from HEK293T cell lysates was performed with 30μL of anti-HA agarose beads (50% slurry, Sigma) or anti-FLAG M2 beads (50% slurry, Sigma).

For overexpression IP in HEK293FT (fast-growing) cells, plasmid cDNA was transfected via Fugene 6 (Promega) (3:1 μL Fugene 6/μg DNA) in serum-free Opti-MEM. 24 hours later the media was aspirated and fresh DMEM culture media was added 24 hr prior to endpoint. At endpoint (48 hours post-transfection), cells were lysed in lysis buffer (20 mM Tris-HCl pH 7.4, 137mM NaCl, 1% Triton X-100, 0.5% sodium deoxycholate, 10% Glycerol, 5mM $MgCl_2$, 2mM EGTA with freshly added 1mM PMSF, 50mM NaF, 1mM Na_3VO_4, 80mM beta-glycerosphosphate plus EDTA-free protease inhibitor cocktail (Roche). After 15–20 min rotating lysis at 4C, lysates were cleared at 20,000g for 20 min at 4C. Cell lysate concentrations were assayed using Advanced Protein Assay Reagent (Cytoskeleton) and then equilibrated with lysis buffer. Lysates were diluted to achieve equal, maximum IP sample concentration and to create Whole Cell Lysate (WCL) samples. 2μg mouse anti-FLAG antibody (Sigma) was added to each IP sample and antibody-lysate solution was rotated for 4 hrs at 4C. 50μL Protein A/G agarose beads (Santa Cruz) were added for 1 hr at 4C to precipitate antibody-antigen complexes. Precipitated complexes were washed three times with lysis buffer for 5 min at 4C, then heated to ≥ 95C for ≥ 5 min in 2X SDS sample buffer (+β-me). The samples were then separated via SDS-PAGE, followed by immunoblotting.

Endogenous Raptor IP

3 10cm cell culture plates of *Tbk1* WT (+/+) or *Tbk1* Δ/Δ MEFs per condition were plated and 2 days later rinsed once in cold PBS. The cells were then lysed in 0.5% NP40-based lysis buffer (50mM Tris HCl, 120mM NaCl, 0.5% NP40, 1mM EDTA, 1mM DTT) or 0.3% CHAPS-based lysis buffer (0.3% CHAPS, 50mM Tris HCl, 120mM NaCl, 1mM EDTA). Post-lysis, protein concentration was equilibrated among samples and equal amounts of protein lysate were added to anti-Raptor antibody-conjugated magnetic beads or anti-FLAG-IgG-conjugated magnetic beads and rotated at 4C for 2 hrs. Beads were then washed 5 minutes (x3) with lysis buffer. Samples were then heated to ≥ 95C for ≥ 5 min in SDS sample buffer (+β-me) and then separated by SDS-PAGE, followed by immunoblotting.

In Vitro Kinase Assay

Recombinant human S6K (Abnova) was first incubated with lambda protein phosphatase in phosphatase buffer (NEB) at a ratio of 3 units of phosphatase per 10ng of protein for 60 min at 30C. Following phosphatase treatment, 100ng of S6K was incubated with or without 50ng recombinant active TBK1 (EMD Millipore) in kinase buffer containing phosphatase inhibitors (25 mM Tris-HCl pH 7.4, 10mM $MgCl_2$, 0.1mM Na_3VO_4, 2mM DTT, 5mM β-glycerosphosphate) in the presence or absence of 200μM ATP for 30 min at 30C (Total reaction volume = 50μL). Kinase reaction was stopped by the addition of 10μL 6X SDS Sample buffer (w/ 10% β-me) followed by heating sample at ≥ 95C for ≥ 5 min. Samples were then separated by SDS-PAGE, followed by immunoblotting.

Scanning Kolmogorov-Smirnov (KS) statistic

A modification to a Kolmogorov-Smirnov (KS) statistic, which we term a scanning ranked KS test, was used to determine which single mutations or co-occurring mutation combinations can best predict a selective sensitivity to BX795. In addition to single mutations, we also annotated a “Ras-Class” metaclass in which we assigned a cell line a value of ‘1’ if it contained a mutation in either *KRAS, NRAS, HRAS, PIK3CA*, or *BRAF*. Mutations or pairwise combinations of co-occurring mutations were first binarized (1=mutated; 0=wild-type), resulting in 184,785 combinations in which at least 5 cell lines contained the mutation combination. For each chemical, we reasoned that if a mutation combination is conferring a selective sensitivity, then the AUC values for cell lines that are mutated will be lower than those that are wild-type. To determine the degree to which the AUC values for cells that are mutated are located towards the bottom of the ranked list sensitivity values, and thus lower than the background distribution, the following equation was used:

$$u = \max_{j=1}^{t} \left[\frac{V(j)}{n} - \frac{(j-1)}{t} \right]$$

where v(j) is the position of each gene in the gene set in the ordered list of genes, t is the total number of cell lines with the mutation combination, and n is the total number of cell lines assayed (n=100). To determine a p-value, 5000 permutations of randomized sorting of ED50/AUC values of size t was performed, and u_{random} was calculated. The resulting p-value was determined to be:

$$p = \frac{\#\text{instances } u_{\text{random}} > u}{\#\text{total permutation}}$$

p<.002 indicates that, out of 5000 permutations, no random value was less than the calculated distance, u. This entire process was repeated for each of the mutation combinations for each compound using AUC values as a sensitivity metric. Our procedure is superior to a standard KS test in several ways. First, when comparing a large distribution to a small distribution in a regular KS test, the NULL hypothesis is biased towards being

rejected. Second, a ranked KS test allows for the preferential ranking of sets that are separated from the background at the tails of the distribution.

Illumina BeadChip Microarray

Raw Illumina HumanWG-6 v3.0 BeadChip files were obtained from the Gene Expression Omnibus using accession number GEO: GSE32036 and normalized as described previously (19).

Elastic Net

Elastic net biomarker identification was performed as in (20,21), with NSCLC cell line mRNA expression values derived from Illumina V3 BeadArrays (GEO: GSE32036). Briefly, the elastic net assigns biomarkers to a response vector of activity scores by solving a basic linear regression problem as follows: Let $X \in \mathbb{R}^{nxp}$ be the matrix of predictive features where n is the number of cell lines included in the training dataset and p is the number of features, and let $y \in \mathbb{R}^{n}$ be the vector of binary sensitivity values for the same cell line panel. Columns of the predictive features matrix and y were normalized to have a mean of zero and a standard deviation of 1. The elastic net attempts to find which weighted linear combination of the columns of the predictive features matrix can best approximate y, or it solves the following equation for w:

$$\mathrm{argmin}_w[\|y - Xw\|_2^2]$$

The elastic net solves the above by enforcing a penalty to the solution that makes the solution both unique and sparse so that only the features that best approximate y are left with non-zero weight values. It does this by combining L1-norm and L2-norm regularization parameters so that the elastic net formulation to the above problem is given by:

$$\mathrm{argmin}_w[\|y - Xw\|_2^2 + \lambda(\alpha\|w\|_2^2 + (1-a)\|w\|_1)]$$

where λ, α are two adjustable parameters such that λ controls the degree of the overall penalty and α controls the degree to which the L1 norm and L2 norm constraints are applied so that when α = 0, only the L1 penalty is applied and when α = 1, only the L2 penalty is applied. In order to determine the optimal values of alpha and lambda to use in the model, we did 100 iterations of 10-fold cross-validation where, in each iteration, the cells were randomly re-sampled into different groups. The values of α and λ were chosen to be those that resulted in the minimum mean squared error for each fold. Features were then chosen to be those with the highest weights that were selected as features in at least 70% of the cross-validation permutations. As input into the elastic net, we used BX795 AUC values from our NSCLC cell lines capped as listed, to find features reporting exceptional response to TBK1 inhibition. The elastic net was run using the glmnet package in R.

S2N comparisons

Cell lines were dichotomized into two groups based on TBK1i sensitivity, where “Ras-Class”-mutant cells with an ED50 < .300 μM were grouped as sensitive and those with

ED50 > 2.5 μM were grouped as resistant. S2N of differentially expressed mRNAs (Source data: GEO: GSE32036) in TBK1i-sensitive vs. TBK1i-resistant NSCLC lines was performed using the following formula: [(meanA - meanB) / (sdA + sdB)], where mean expression of mRNA "x" in cell line group B is subtracted from mean of mRNA "x" in cell line group A, and then divided by the sum of the standard deviations (sd) of "x" in groups A and B. This was then followed by a hypergeometric test (via "phyper" function in R) to determine significance of overlap between top and bottom 5% most differentially expressed mRNAs among the TBK1i-treated lines and the genes comprising the EMT gene signatures (22,23).

TBK1 Inhibitor Sensitivity vs. Gene Expression Correlations

TBK1 inhibitor sensitivity (ED50 or AUC) from 93 NSCLC cell lines were Log_{10}-transformed and plotted against Log_2 mRNA expression of Ras-effector or EMT network gene subsets, as annotated in Table S3. Plots, linear regression best-fit lines, and statistical analyses were generated using GraphPad Prism. *P < 0.05, **P < 0.01, ***P < 0.001, ****P < 0.0001 (See also Table S3). Source data: GEO: GSE32036. For the cumulative distribution analyses for EMT-related gene sets, the ks.test function in R was used to compare the overall mRNA expression (Log_2) of *ZEB1*-repressed epithelial genes (24) (KS-test p-value = 9.951e-09) or epithelial state gene markers (23) (KS test P value = < 2.2e-16) in "Ras-Class"-mutant/TBK1i-sensitive (HCC15, H324, H1299, HCC44, H157, H1155) vs. "Ras-Class"-mutant/TBK1i-resistant (H2347, H1573, H650, H441, HCC2450, H596, HCC4019, H2887) NSCLC cell lines. Source data: GEO: GSE32036 NSCLC cell line mRNA expression data for the genes listed in the relevant figures.

EMT-modulation of TBK1 Sensitivity

NSCLC cells were plated in 96-well cell culture plates and subsequently treated with DMSO or TBK1 inhibitors (BX795 or Compound II) for 72 hrs. Cell viability was assayed post-treatment via Cell-Titer Glo (Promega). For TGF-beta-treated cells, NSCLC lines were first cultured in RPMI-5%FBS +antibiotics + 2ng/mL recombinant TGF-beta (Peprotech, 100-21) for 1–2 weeks prior to compound treatment and viability assays. For "Post"-TGF-beta conditions, TGF-beta-treated cells were re-cultured in TGF-beta-free RPMI-5% +antibiotics media for greater than 1 week prior to compound treatment and viability assays.

Caspase 3/7 (Caspase Glo) Assay

For each cell line, 2000 cells were plated in 100μL RPMI (0.5% FBS)/well in 96-well cell culture plates. Approximately 15 hrs later, media was changed with serum-free RPMI or RPMI (+10ng/mL recombinant TGF-beta [Peprotech, 100-21]) for 24 hrs. DMSO or Compound II was then added to the final concentrations listed for 24 hrs. At endpoint, 100μL Caspase Glo (Promega) complete reagent was added and incubated for 30 min at RT. Luminescence was then measured via PheraStar FS plate-reader.

Compound II inhibition of TGF-beta-dependent EMT gene expression

500,000 A549 cells were plated in 6-well cell culture dishes and the following day, 0.1% DMSO, 0.5μM Compound II or 2μM Compound II were added for 30 min, after which

10ng/mL recombinant TGF-beta (Peprotech, 100-21) was added for 24 hrs. Cells were then washed with PBS and then collected into PBS and pelleted via bench top centrifuge. Cell pellets were lysed and RNA was collected via RNeasy Kit (Qiagen). mRNA was reverse transcribed into cDNA and relative transcript abundance was measured by Taqman-qPCR probe sets (Applied Bio-Science).

Statistical Analyses

Statistical analyses were conducted using either R (Versions 3.3.0, 3.3.1, and earlier. R Foundation for Statistical Computing, Vienna, Austria) or GraphPad Prism (Versions 6 or 7), as indicated in the relevant Figure Legend and/or Methods section. Comparisons between conditions were conducted using Student's *t* test or one-way ANOVA, as indicated in the relevant Figure Legend and/or Methods section. Statistical significance is defined as $P < 0.05$.

Results

Chemical breadth of efficacy screens in NSCLC lines indicate extensive correlation between TBK1 and AKT/mTOR inhibitor sensitivity

To begin to decipher the nature of selective cell autonomous sensitivity to TBK1 activity, we profiled two structurally distinct small molecule ATP-competitive TBK1 (and IKKe) inhibitors (BX795 and the 6-amino pyrozolopyrimidine Compound II (5,25)) via 12-point compound dose-response curves (50 p*M* – 50 μ*M*) in 100 NSCLC cell lines (Figures 1A–B, Table S1). Both inhibitors displayed a broad range of activity (> 2 logs) that was significantly correlated as a function of mean ED50 or area-under-the-curve (AUC) (Figures 1C–D). The observed cell-selective sensitivity profiles did not simply correlate with cell-proliferation rates, suggesting distinct biology may underpin TBK1-dependency (Figures 1E–F). Two independent large-scale, cell-based chemical profiling efforts (16,17) were queried to identify additional well-characterized chemicals with similar activity profiles. For this analysis, proliferation inhibition activity scores (ED50 or AUC) for the TBK1 inhibitors BX795 and Compound II were plotted against the activity scores for all other chemicals tested within the subsets of NSCLC cell lines treated with the relevant compounds. Pearson correlation values were calculated for all pairwise comparisons and compounds were ranked by their correlation with TBK1 inhibitors (TBK1i) (1 = maximum equivalence). We then asked if any biochemical signaling pathways were enriched among the best correlating compounds. This effort returned a consistent positive correlation between TBK1i and compounds targeting the AKT/mTOR signaling pathway (Figures 1G–I, Table S2). One characterized inhibitor of TBK1 (Momelotinib or CYT387, a TBK1/IKKe/JAK inhibitor (26)) was screened in (17) and it displayed a robust correlation with our TBK1i data (Figure 1J), lending confidence that the data sets were queried in a reasonable manner. The AKT/mTOR pathway inhibitor correlations are reminiscent of the reported role of TBK1 in direct activation of AKT in some contexts (4,5,27), and suggest shared cell-autonomous sensitivities to inhibition of TBK1 and inhibition of AKT/mTORC1 signaling. Also, consistent with a suspected role of TBK1-mediated AKT activation to support mutant *KRAS*-mediated oncogenesis (4,5), we observed consistent positive correlation between TBK1i and AKT/mTORC1 pathway inhibitors among *KRAS*-mutant NSCLC lines (Figures

1K–N, Table S2). Correlations within the *KRAS*-mutant subpopulation exceeded those among the full NSCLC panel (Figures 1K–N), suggesting a mechanistic relationship between TBK1 and AKT/mTORC1 signaling may be particularly relevant for the survival of *KRAS*-mutant NSCLC cells. From a shotgun phosphoproteomics resource (28), we noted that depletion of *TBK1* in NSCLC can perturb phosphorylation of multiple nodes in the AKT/mTORC1 signaling network (Figure 1O), which suggests a mechanistic relationship between TBK1 and mTORC1 activation may underlie shared sensitivities of cancer cell lines to TBK1/IKKe and mTOR pathway inhibition. Consistent with this possibility, overexpression of TBK1 was sufficient to induce mTOR auto-phosphorylation (pS2481) in a TBK1 kinase activity-dependent manner (Figure 1P).

TBK1 supports AKT/mTORC1 activation during an amino acid starved-to-fed state transition

The mammalian target of rapamycin (mTOR) is a master regulator of protein translation and cell growth. Within mTOR complex 1 (mTORC1), mTOR activity is acutely responsive to cellular availability of carbon sources and essential amino acids (EAA) (29). To directly assess participation of TBK1 in support of mTORC1, we first modeled the consequence of deletion or depletion of TBK1 on nutrient-dependent activation of mTORC1. An amino acid starved-to-fed state transition was optimized to produce a large dynamic range of response to stimulus in culture as indicated by accumulation of activating phosphorylation on the mTORC1 substrate p70 S6 Kinase (S6K) (pT389) (Figure S1A). Mouse embryonic fibroblasts (MEFs) with homozygous deletion of *Tbk1* displayed significant blunting of nutrient stimulated mTORC1 activation as compared to matched wild-type controls (Figure 2A), which was also associated with reduced accumulation of phospho-AKT (pT308 and pS473). While homozygous deletion of *Tbk1* is embryonic lethal (30), mice harboring a translated homozygous N-terminal truncation of the *Tbk1* kinase-domain are viable (15). mTORC1 pathway activity was intact in MEFs derived from homozygous mutant (Δ/Δ) animals and cultured in serum-replete media, but was almost completely non-responsive to amino acid stimulation as compared to MEFs derived from WT or heterozygous mutant (+/Δ) animals (Figure 2B). Residual baseline AKT/mTORC1 activation in *Tbk1* (Δ/Δ) MEFs was sensitive to mTOR inhibitors suggesting TBK1 modulates, but does not explicitly determine, mTORC1 activation (Figures S1B–C). Moreover, transient depletion of *TBK1* in cancer cell lines (MNT1 and HCT116) also blunted AKT and S6K phosphorylation in response to amino acid stimulation (Figures 2C–D). Finally, three structurally distinct TBK1 inhibitors, the 6-amino pyrozolopyrimidine Compound II, BX795, and an experimental TBK1/IKKe inhibitor developed by Glaxo-Smith-Kline (GSK2292978A, aka GSK) (AACR-NCI-EORTC Poster by Richter, et. al., 2009) (Figure S1D), attenuated amino acid-induced mTORC1 pathway activation in immortalized MEFs (Figure 2E). As BX795 has significant activity against the AKT regulatory kinase PDK1 in addition to TBK1/IKKe (25), we also tested BX795 in *PDPK1*-null (−/−) colorectal carcinoma cells (HCT116). Here, we observed equivalent blunting of mTORC1 and AKT activation by BX795 independently of the presence of *PDPK1* (Figure 2F). Together, these observations indicate that TBK1 supports activation of AKT/mTORC1 signaling during an amino acid starved-to-fed state transition.

Immunoprecipitation (IP) of endogenous TBK1 resulted in a co-precipitation of endogenous mTOR, that was enriched by amino acid stimulation in a time-dependent manner, suggesting TBK1 is physically associated with an mTOR regulatory complex (Figure 3A). Additionally, nutrient-induced positive feedback phosphorylation of mTOR (pS2448) by S6K in these complexes suggested that TBK1 associates with a subset of mTORC1 that is directly responsive to nutrient availability. Previous work has defined multi-subunit exocyst complexes as direct modulators of both TBK1 (6), and mTORC1 kinase activity (31). Although not previously explored, these findings suggest a guilt-by-association molecular interaction between TBK1 and mTORC1 via shared exocyst complexes. Consistent with this, affinity-tag precipitation of wild-type (WT) or kinase-dead (KD) TBK1 co-precipitated endogenous components of the exocyst (Sec5, Exo70) together with mTORC1 (mTOR, Raptor) and mTORC1 positive and negative regulators (AKT, TSC2) (Figure 3B). mTOR and AKT in the WT TBK1 complexes were responsive to amino acid stimulation in a time dependent manner; however KD TBK1, though maintaining association with mTOR and AKT, was dominant inhibitory to their activation. Notably, RNAi-mediated depletion of some, but not all, known TBK1 interactors (e.g. AZI2, NEMO, AKT, exocyst subunits) (Figure S2) inhibited nutrient-dependent mTORC1 signaling similar to depletion of TBK1 alone (Figures 2C–D), indicating the participation of TBK1 regulatory machinery in nutrient-dependent activation of mTORC1.

TBK1 is physically associated with multiple AKT/mTOR regulatory elements

Quantitative analysis of TBK1 complexes via immunoprecipitation/mass spectrometry returned both the mTORC1-specific subunit Raptor and the mTORC1 downstream effector S6K among the strongest TBK1-specific interactors (Figure 3C, Upper). The interaction of TBK1 with S6K was validated by a reverse co-expression/co-IP (Figure 3D), and we reasoned the detected association may be a consequence of the presence of TBK1 in a stable mTORC1 activator/effector complex. Moreover, a proteome-wide analysis of TBK1-dependent phosphopeptides in lung cancer cells reported decreased phosphorylation of S6K (Thr 421/Ser 424) upon genetic depletion of *TBK1* (Figure 3C, Lower, modified from (28)). These residues are not the canonical mTOR substrate site (pT389), but rather reside within a C-terminal autoinhibitory domain in S6K (32), suggesting TBK1 may directly influence S6K activity. This same analysis returned decreased phosphorylation of known TBK1 substrates AKT and p62 at currently uncharacterized sites (pT451 and pS212, respectively). Also observed were predicted indirect consequences of TBK1 loss on phosphorylation of AKT and mTOR effectors, TSC2, Ribosomal Protein S6, and 4EBP1. Additionally, decreased phosphorylation of mTORC1 inhibitory interactor Raptor in this same analysis paralleled an amino acid-induced increase in total Raptor within TBK1 complexes (Figure 3B), to which KD TBK1 overexpression was dominant inhibitory. These observations, together with decreased phosphorylation of identical regions within mTORC1 regulatory subunits RagC and RagD, collectively point to TBK1 as potentially supporting AKT/mTOR signaling via multiple molecular mechanisms.

To test this, we first further examined the Rag family of GTPases, which mediate mTORC1 activation by amino acids in cooperation with the Ragulator complex at lysosomes (33), for potential isoform-specific associations with TBK1. Bi-directional IPs of ectopically

expressed Rag GTPases (Figure 3E) or TBK1 (Figure 3F) showed strong and selective association of TBK1 with RagD in a manner that was non-competitive with RagC or RagD interactions with endogenous mTOR (Figure 3E). Rag proteins typically operate in cells as heterodimers, in which RagA or RagB pairs with RagC or RagD. Expression of RagA reduced RagD association with TBK1, while expression of RagB enhanced it, suggesting preferential affinity of TBK1 for RagB/D Heterodimers (Figure 3G). This was observed irrespective of the nucleotide-bound states of RagD (GDP-bound (77L) or GTP-bound (121L)) (Figure 3H), suggesting the potential for constitutive association of a subset of TBK1 within RagD complexes that is independent of cellular nutrient status.

TBK1 supports mTORC1 pathway activation both upstream and downstream of mTOR

Given evidence for multiple points of interaction of TBK1 with canonical components of mTORC1 and its regulatory elements, we next examined the potential relevance of these associations to mTORC1 pathway activation. A direct context-selective activation of AKT by TBK1 has been previously defined by three independent groups (4,5,27). To directly assess the extent to which this accounts for TBK1-dependent mTORC1 activity, we first examined whether TBK1's contribution to mTORC1 was fully or partially AKT-dependent. Exposure of *PDPK1* −/− HCT116 cells to BX795 (to inhibit TBK1) or MK2206 (an allosteric AKT inhibitor), either alone or in combination, resulted in equivalent inhibition of phospho-S6K (pT389) upon nutrient stimulation, consistent with the hypothesis that TBK1 regulation of mTORC1 is AKT-dependent (Figure 4A). Moreover, inhibition of mTORC1 activity by TBK1 inhibition correlated with loss of AKT substrate site phosphorylation on PRAS40 (pT246), a direct negative regulator of mTORC1 (Figures 2D and 4A). Phosphorylation of PRAS40 (T246) promotes dissociation of PRAS40 from Raptor, which corresponds to increased mTORC1 activity (33). Consistent with this, we found that loss of TBK1 activity in *Tbk1* (Δ/Δ) MEFs corresponded to increased association of PRAS40 with Raptor, commensurate with a TBK1-dependent phosphorylation of PRAS40 by AKT (Figure 4B, Left). This enhanced interaction was robustly maintained under detergent conditions (Figure 4B, Right) reported as sufficient to disrupt mTOR/Raptor interactions (34). Finally, we noted that the constitutively active mTORC1 phosphorylation of S6K (T389) in *Tsc2*-null cells is relatively insensitive to TBK1 inhibitors (Figure 4C).

The above strongly indicate that TBK1-dependent mTORC1 activation occurs predominantly as a consequence of TBK1-dependent activation of AKT. However, we noted that phosphorylation of the carboxy-terminal tail of S6K (T421/S424) was perturbed in cases where TBK1 was genetically or chemically inhibited (Figures 4C–D), including within a *Tsc2*-null background (Figure 4C). Phosphorylation of S6K at these sites is reported to relieve C-terminal autoinhibitory domain repression of kinase activity (32). Though mitotic arrest-activated Cdc2 (35) and TNFα-stimulated JNK1 (36) are reported as kinases for these sites, it is an open question as to which mechanisms govern T421 and S424 phosphorylation in response to amino acid availability. Given evidence for a physical association between S6K and TBK1 (Figures 3C–D), and the consistent functional consequences of TBK1 inhibition on S6K phosphorylation, we considered the possibility that TBK1 may promote mTORC1 pathway activation both upstream (via AKT) and downstream (via S6K) of mTOR itself. Consistent with this hypothesis, we found that TBK1 expression promotes S6K

phosphorylation (T421/S424) within TBK1/S6K complexes in a TBK1 kinase-dependent manner (Figure 4E). Furthermore, purified recombinant TBK1 was sufficient to directly phosphorylate purified recombinant S6K on T421/S424 *in vitro* (Figure 4F). These collective observations suggest TBK1 supports nutrient-dependent mTORC1 activation and function through multiple physical and functional interactions (Figure 4G).

Identification of a TBK1-dependent Molecular Subtype of NSCLC Cells

We next sought to determine the nature of the biological context that is associated with cell-autonomous addiction to TBK1 activity by identifying potential mutation-based biomarkers that indicate cancer cell-intrinsic TBK1-dependence. Gene-level non-synonymous variants in each of 94 NSCLC cell lines were identified with whole exome sequencing. For candidate biomarker discovery, we selected the subset of genes mutated in at least 5 cell lines. Using a modification to a standard Kolmogorov-Smirnov (KS) statistic, we scanned the resulting 4139 single gene mutations, 180,646 pairwise combinations of co-occurring mutations, and curated gene sets corresponding to key cancer pathways, to rank those that predict the best sensitivity to BX795. This automated approach returned mutations in *KRAS, HRAS, NRAS, PIK3CA*, or *BRAF* (members of a “Ras-Class”) as significantly associated with sensitivity to TBK1 inhibition (Figure 5A). This enriched sensitivity distribution remained intact if the molecular characteristic was strictly defined by *KRAS* mutation alone, though significance is reduced (Figure S3A). *KRAS* expression also correlated with *KRAS*-mutant cell sensitivity to TBK1i (Figure S3B); however, it was evident that oncogenic *KRAS* expression is an insufficient single mechanistic distinction between TBK1i-sensitive and -resistant *KRAS*-mutant lines. (Figures 5A, S3A–B). Consistent with this, we found that selective inhibition of AKT/mTOR pathway activity by short-term TBK1 inhibition was coupled to selective toxicity of long-term TBK1 inhibition among *KRAS*-mutant NSCLC lines (Figure 5B). Of note, this observation was concordant with the positive correlation between sensitivity to TBK1 and AKT/mTOR pathway inhibitors in the NSCLC cell line panel (Figures 1K–N), and suggests addiction to TBK1-dependent support of AKT pathway activation is the mechanistic basis of that correlation.

To potentially parse the additional molecular features that correspond to “Ras-Class”-mutant/TBK1-dependent cell states, we used a penalized linear regression machine learning procedure (elastic net) to associate additional features that can specify sensitivities to TBK1i (20,21). This analysis returned a quantitative 4-gene signature derived from Illumina V3 BeadArray NSCLC mRNA expression microarray (GEO: GSE32036) (Figure 5C). Of note, within this signature, high *ZEB1* expression (approximately 16-fold over baseline) was enriched in the TBK1i-sensitive subpopulation of NSCLC cell lines. ZEB1 is one of several transcription factors that promote the epithelial-to-mesenchymal transition (EMT) that is a characteristic of aggressive, therapy-refractory tumors (37). In the context of *KRAS*-mutant lung carcinoma, differential requirement of KRAS itself corresponds to distinct epithelial or mesenchymal subtypes, in which *KRAS*-mutant NSCLC that have undergone EMT are no longer KRAS-addicted (22). Given the potential link between TBK1i sensitivity and EMT suggested by the *ZEB1* biomarker, and the multiple mechanistic links between AKT/mTOR signaling and EMT (38), we examined the degree to which mesenchymal versus epithelial status stratified TBK1i-sensitive versus TBK1i-resistant “Ras-Class”-mutant NSCLC

(Figures 5D, S3C). We stratified “Ras-Class”-mutant NSCLC into two categories, based on TBK1i responsiveness, and then ranked genes differentially enriched in each category with a signal to noise metric. Indeed, genes enriched in the “Ras-Class”-mutant/TBK1i-sensitive subclass significantly overlapped with genes that correspond to *KRAS*-mutant/mesenchymal NSCLC (hypergeometric p = 2.3E-7) and those enriched in the “Ras-Class”-mutant/TBK1i-resistant subclass significantly overlapped with genes that correspond to *KRAS*-mutant/epithelial NSCLC (hypergeometric P = < 1.6e-16) (Figure 5D) (22). This association was reproduced with two independent gene signatures that parse epithelial versus mesenchymal status (23,39) (Figures S3D–E). Furthermore, across the NSCLC panel, TBK1i AUC significantly anti-correlated with pro-mesenchymal state genes, *ZEB1, ZEB2* and *SNAI1*, and positively correlated with epithelial marker, *CDH1* (Figure 5E, Table S3). Consistent with *ZEB1*’s role as a transcriptional repressor of expression programs otherwise promoting epithelialization, we found that expression of *ZEB1*-repressed epithelial genes (24), as well as epithelial markers in general (23), was significantly reduced (p-value = 9.951e-09, and P value = < 2.2e-16) in “Ras-Class”-mutant/TBK1i-sensitive lines (Figures 5F–G). These cumulative observations indicate that mesenchymal “Ras-Class”-mutant NSCLC cells are selectively dependent on TBK1 activity.

Modulation of Mesenchymal Status is Sufficient to Alter *KRAS*-Mutant NSCLC Sensitivity to TBK1 Inhibitors

We next asked if mesenchymal status is mechanistically coupled to TBK1-dependent support of cancer cell survival. To test this, we first evaluated the consequence of inducing a mesenchymal to epithelial state transition on TBK1-dependence for cell survival. The *KRAS*-mutant/*LKB1*-mutant genotype in NSCLC is associated with mesenchymal features *in vivo* and in culture (21,40) and LKB1 activity is a major determinant of epithelialization (41). Therefore, we leveraged this background to induce a mesenchymal-to-epithelial transition by stable overexpression of WT LKB1 in an otherwise TBK1-dependent, mesenchymal/*KRAS*-mutant cell line (HCC44; *KRAS*-mutant/*LKB1*-mutant and TBK1i-sensitive) (Figure S4A). This corresponded to a measurable (greater than two-fold) reduction of sensitivity to TBK1 inhibition in an LKB1 kinase-dependent-manner (Figure S4B), suggesting a mesenchymal phenotype may drive sensitivity to TBK1 in the context of Ras mutations.

Transforming Growth Factor Beta (TGF-beta) is a potent inducer of EMT that promotes the survival and migration of cancer cells (38). Of note, we found that Functional Signature Ontology (FUSION)-derived similarity clustering of siRNA and miRNA effects on reporter gene expression (42) saw *TBK1* siRNA cluster most closely with siRNA against TGF-beta Receptor 2 (*TGFBR2*), as a function of both Pearson correlation and Euclidean distance (Figures 6A, S4C). This tool ranks the similarity of genetic perturbations on cell behavior to generate guilt-by-association hypotheses, and therefore indicates that depletion of *TBK1* or *TGFBR2* results in highly similar phenotypes. Furthermore, *TBK1, RALBP1* (a canonical RalA/B effector), and *TGFBR2* emerged from an array of >4000 shRNAs (43) as among the gene targets whose depletion most tightly correlated with TBK1i sensitivity in 18 NSCLC cell lines (Figure 6B). Intriguingly, expression of *TGFBR2* and its ligand *TGFB1* also significantly anti-correlated with TBK1i ED50s in the NSCLC panel (Figure S4D, Table

S3). Given these multiple independent correlates linking TBK1 and TGF-beta signaling, we chose TGF-beta-mediated induction of mesenchymal characteristics to test if EMT is sufficient to sensitize *KRAS*-mutant NSCLC lines to TBK1 inhibitors. Among those cell lines tested, TGF-beta signaling in A549 was highly responsive to recombinant TGF-beta as indicated by phosphorylation of the TGFBR2 effector SMAD2 and a clear switch from epithelial to mesenchymal protein markers (Figure 6C). Accordingly, recombinant TGF-beta selectively sensitized A549 to both BX795 and Compound II (Figures 6D–E, S4E–F). Expression analysis of a panel of TGF-beta-responsive EMT markers post-exposure to TBK1 inhibitors identified *SNAI1*, a key EMT early response gene (38), as partially dependent on TBK1 activity (Figure 6F). More latent EMT genes were not significantly affected (Figure S4G). Finally, induction of TGF-beta signaling and EMT was reversible by re-culture of TGF-beta-adapted A549 cells in TGF-beta-free media, which also reversed sensitivity to TBK1 inhibition (Figure 6D, “Post TGFb”). These combined observations support a context-selective mechanism whereby, in Ras-mutant/mesenchymal NSCLC cells, TBK1 supports activation of AKT/mTOR concomitant with sustaining a TGF-beta/EMT phenotype (Figure 6G)

Discussion

Accumulating observations link activity of the atypical IκB serine/threonine protein kinase TBK1 to diverse, but potentially interconnected, cellular activities engaged by distinct TBK1 substrates. These include activation of type I interferons (IFN), support of endosome osmotic integrity, clearance of autophagic substrates, induction of mitogenic responses, regulation of cell shape, modulation of apoptosis, and induction of protein synthesis and cell growth (5–10,13,30,44–46). These activities, by extrapolation, are individually or combinatorially associated with the consequences of TBK1 dysregulation on developmental disorders, inflammatory disease, and neoplastic disease (11–13). Given TBK1’s broad sphere of functional influence, we initiated the current study to deconvolve the context-selective role of TBK1 in cancer cell survival. Using broad-scale chemogenomic and interactome discovery strategies, we uncovered evidence that TBK1 supports AKT/mTORC1 pathway activation through direct engagement of multiple pathway components acting both upstream and downstream of the mTOR kinase itself. Furthermore, we identified distinct molecular features that robustly specify a cancer cell biological context that is dependent on TBK1 support of AKT/mTORC1 pathway activation for survival.

Previous work, directly relevant to the studies presented here, demonstrated that TBK1 is responsible for activating phosphorylation of AKT via exocyst complexes and is required for context-selective AKT activation (4,5,27). Collective consideration of observations separately linking mTOR and TBK1 to distinct exocyst subunits (6,31) implied these kinases may reside together in exocyst complexes, which was, in fact, observed in this study (Figure 3B). The mechanistic relevance of these associations was indicated by the blunting of mTORC1 signaling upon exocyst subunit depletion (Figure S2). The physical association of TBK1 with multiple mTORC1 regulatory elements including Raptor, RagD, and S6K indicates that TBK1 may play heretofore unappreciated roles in the regulation of additional processes governing AKT/mTOR signaling, such as Rag GTPase function, mTOR localization, or direct nutrient sensing (33). Notably, we show here for the first time that

TBK1 can directly promote S6K C-terminal T421/S424 phosphorylation. According to prevailing evidence, S6K is first phosphorylated on these C-terminal autoinhibitory domain residues as a priming step that induces a conformational change that allows subsequent activating phosphorylation of S6K at the hydrophobic motif within its linker domain (pT389, by mTOR) and/or the T-loop of its kinase domain (pT229, by PDK1) (32). This mechanism suggests that, from within a multi-protein complex, TBK1 can influence S6K activation though a dual mechanism of direct priming phosphorylation of S6K, by TBK1 itself, and indirect activating phosphorylation of S6K via mTORC1.

Control of the activation and substrate-specificity of TBK1 is likely to be heavily influenced by selective adaptor engagement and subcellular localization (47). For example, TBK1 is recruited by TRAF-mediated ubiquitination of MAVS or TRIF to mediate innate immune responses to viral RNA-sensing by RIG-1 or bacterial LPS-sensing by TLR4, respectively (44). Furthermore TBK1 is directly engaged in response to cytosolic DNA-sensing by its association with S6K/STING complexes downstream of cGAS (44,48). Within these stimuli-specific complexes, TBK1 phosphorylates adaptor proteins to recruit IRF3 for subsequent phosphorylation by TBK1, allowing IRF3 homodimerization and translocation to the nucleus to induce type I interferons (44). TBK1 can be independently engaged to promote selective autophagy of ubiquitinated cargo by phosphorylating ubiquitin-binding autophagy adaptors such as Optineurin (9) or p62 (SQSTM1) (49). Notably, TBK1 associates with distinct adaptor proteins at discrete subcellular compartments, which likely contributes to its selective support of distinct biological systems. For example, TBK1 can interact with STING at perinuclear endosomal compartments also containing Sec5 (50). In addition, TBK1 adaptors Nap1 (*AZI2*), Sintbad (*TBKBP1*), or TANK all displayed dissimilar subcellular localization in a study of TBK1 network engagement (51). While our work, and related observations, suggest the TBK1/S6K regulatory relationship can support survival of some cancer cell types, these observations may also have important mechanistic implications for S6K-dependent innate immune signaling within the STING-TBK1 pathway (48).

Using machine-automated association analysis of chemical response profiles with quantitative genomic features, we identified a mesenchymal subtype of *KRAS*-mutant lung cancer cells as distinctly sensitive to perturbation of TBK1 kinase-dependent support of AKT/mTOR pathway activation and cell survival. This “molecular subtype” of NSCLC has been previously noted to correspond to aggressive therapy refractory disease and resistance to MEK pathway inhibition *in vitro* and *in vivo* (21,22,40). Experimental recapitulation of this subtype via loss of function *LKB1* alterations in *KRAS*-mutant backgrounds has been demonstrated *in vitro* and *in vivo* (21,40,52), and was shown to be sufficient to modulate response to TBK1 inhibition in this study. SRC tyrosine kinase activity has been nominated as an upstream mechanistic driver of the tumorigenic properties of this subtype (40). This finding, coupled with the striking observation that SRC directly induces Y179 phosphorylation on TBK1 to promote TBK1 autoactivation in response to viral infection (53), suggests a SRC-TBK1-AKT/mTOR cascade may be corrupted to promote cell survival in the context of mesenchymal *KRAS*-mutant lung cancer.

TGF-beta is a well-appreciated master regulator of epithelial to mesenchymal transition and can make highly context-selective contributions to cancer cell survival (38). These activities

have multiple points of mechanistic intersection with AKT/mTOR signaling that, as shown here, are likely integrated with and to some extent dependent upon TBK1 activity (Figure 6G). Substantial related work is also consistent with this notion. For example, TGF-beta induction of cell migration utilizes the same RalB/exocyst (Sec5) machinery (54) that also promotes TBK1 and AKT activation in response to KRAS activation and host defense pathway (TLR3) activation (5,6). Furthermore, TBK1 inhibition attenuates AKT phosphorylation of Glycogen Synthase Kinase 3 alpha/beta (GSK3-a/b) at S21/9 and overexpression of TBK1 is sufficient to induce GSK3-b phosphorylation by AKT in a TBK1 kinase-dependent manner (5). This phosphorylation of GSK3-b by AKT supports EMT by blocking GSK3-b-mediated SNAIL phosphorylation and cytosolic sequestration (38). In response to TGF-beta signaling, SNAIL promotes expression of pro-EMT transcription factor, *ZEB1*, a key biomarker of TBK1-addiction that is also TBK1-responsive (38,55). Finally, a systems-level analysis of a functional signature-derived similarity matrix of kinases and miRNAs (42) returned strong connections among the miR-200 family activation, TBK1 inhibition, and TGF-beta inhibition. The miR-200 family is well appreciated for its role in suppressing EMT through destabilization of *ZEB1* mRNA (38)

Taken together, these observations suggest that TBK1 supports key, context-specific tumorigenic activity in Ras-mutant/mesenchymal NSCLC. As approximately 30% of human cancers harbor activating mutations in Ras isoforms (1), the dissection of TBK1-sensitive subpopulations of “Ras-class”-mutant NSCLC adenocarcinoma may shed light on possible therapeutic applications for cancers of the lung, colon, and pancreas. As mesenchymal cell fate phenotypes are associated with aggressive disease and poor patient outcomes (37), discovery that “Ras-class”-mutant/mesenchymal cancer cell lines are selectively sensitive to TBK1 inhibitors nominates TBK1-signaling for consideration as a target in the treatment of this cadre of patients with limited therapeutic options.

Supplementary Material

Refer to Web version on PubMed Central for supplementary material.

Acknowledgments

We thank John Minna, Adi Gazdar, Rolf Brekken, James Brugarolas, Seng-Lai "Thomas" Tan, Xuetao Cao, Kun-Liang Guan, Michael Marks, Charles Yeaman, Shu-Chan Hsu, William Hahn, and Bert Vogelstein for several of the reagents employed in these studies. We are grateful to Ralph DeBerardinis for NSCLC growth rate data. We also thank Rolf Brekken, Victoria Cruz, and the members of the White laboratory for invaluable advice and discussion. M.A.W. is currently Chief Scientific Officer and Vice President of Tumor Cell Biology at Pfizer, Inc.

Grant Support

This work was supported by the National Institutes of Health (CA142543, UTSW Cancer Center Support Grant supporting B.A. Posner; CA071443, CA197717, and CA176284, awarded to M.A. White.) and The Welch Foundation (I-1414, awarded to M.A. White.).

References

1. Lu S, Jang H, Gu S, Zhang J, Nussinov R. Drugging Ras GTPase: a comprehensive mechanistic and signaling structural view. Chem Soc Rev. 2016; 45:4929–52. [PubMed: 27396271]
2. Cooper JM, Bodemann BO, White MA. The RalGEF/Ral pathway: evaluating an intervention opportunity for Ras cancers. Enzymes. 2013; 34(Pt B):137–56. [PubMed: 25034103]

3. Gentry LR, Martin TD, Reiner DJ, Der CJ. Ral small GTPase signaling and oncogenesis: More than just 15minutes of fame. Biochim Biophys Acta. 2014; 1843:2976–88. [PubMed: 25219551]
4. Xie X, Zhang D, Zhao B, Lu M-K, You M, Condorelli G, et al. IkappaB kinase epsilon and TANK-binding kinase 1 activate AKT by direct phosphorylation. Proc Natl Acad Sci USA. 2011; 108:6474–9. [PubMed: 21464307]
5. Ou Y-H, Torres M, Ram R, Formstecher E, Roland C, Cheng T, et al. TBK1 directly engages Akt/PKB survival signaling to support oncogenic transformation. Molecular Cell. 2011; 41:458–70. [PubMed: 21329883]
6. Chien Y, Kim S, Bumeister R, Loo Y-M, Kwon SW, Johnson CL, et al. RalB GTPase-mediated activation of the IkappaB family kinase TBK1 couples innate immune signaling to tumor cell survival. Cell. 2006; 127:157–70. [PubMed: 17018283]
7. Perry AK, Chow EK, Goodnough JB, Yeh W-C, Cheng G. Differential requirement for TANK-binding kinase-1 in type I interferon responses to toll-like receptor activation and viral infection. J Exp Med. 2004; 199:1651–8. [PubMed: 15210743]
8. Sharma S, tenOever BR, Grandvaux N, Zhou G-P, Lin R, Hiscott J. Triggering the interferon antiviral response through an IKK-related pathway. Science. 2003; 300:1148–51. [PubMed: 12702806]
9. Wild P, Farhan H, McEwan DG, Wagner S, Rogov VV, Brady NR, et al. Phosphorylation of the autophagy receptor optineurin restricts Salmonella growth. Science. 2011; 333:228–33. [PubMed: 21617041]
10. Radtke AL, Delbridge LM, Balachandran S, Barber GN, O'Riordan MXD. TBK1 protects vacuolar integrity during intracellular bacterial infection. PLoS Pathog. 2007; 3:e29. [PubMed: 17335348]
11. Barbie DA, Tamayo P, Boehm JS, Kim SY, Moody SE, Dunn IF, et al. Systematic RNA interference reveals that oncogenic KRAS-driven cancers require TBK1. Nature. 2009; 462:108–12. [PubMed: 19847166]
12. Freischmidt A, Wieland T, Richter B, Ruf W, Schaeffer V, Müller K, et al. Haploinsufficiency of TBK1 causes familial ALS and fronto-temporal dementia. Nat Neurosci. 2015; 18:631–6. [PubMed: 25803835]
13. Hasan M, Yan N. Therapeutic potential of targeting TBK1 in autoimmune diseases and interferonopathies. Pharmacol Res. 2016; 111:336–42. [PubMed: 27353409]
14. Sharpless, NE. Cell Biology, Four-Volume Set. Vol. 1. Elsevier Inc; 2006. Preparation and immortalization of primary murine cells; p. 223-228.Available from
15. Marchlik E, Thakker P, Carlson T, Jiang Z, Ryan M, Marusic S, et al. Mice lacking Tbk1 activity exhibit immune cell infiltrates in multiple tissues and increased susceptibility to LPS-induced lethality. Journal of Leukocyte Biology. 2010; 88:1171–80. [PubMed: 20651301]
16. Garnett MJ, Edelman EJ, Heidorn SJ, Greenman CD, Dastur A, Lau KW, et al. Systematic identification of genomic markers of drug sensitivity in cancer cells. Nature. 2012; 483:570–5. [PubMed: 22460902]
17. Seashore-Ludlow B, Rees MG, Cheah JH, Cokol M, Price EV, Coletti ME, et al. Harnessing Connectivity in a Large-Scale Small-Molecule Sensitivity Dataset. Cancer Discovery. 2015; 5:1210–23. [PubMed: 26482930]
18. Trudgian DC, Ridlova G, Fischer R, Mackeen MM, Ternette N, Acuto O, et al. Comparative evaluation of label-free SINQ normalized spectral index quantitation in the central proteomics facilities pipeline. Proteomics. 2011; 11:2790–7. [PubMed: 21656681]
19. Kim J, McMillan E, Kim HS, Venkateswaran N, Makkar G, Rodriguez-Canales J, et al. XPO1-dependent nuclear export is a druggable vulnerability in KRAS-mutant lung cancer. Nature. 2016; 538:114–7. [PubMed: 27680702]
20. Potts MB, McMillan EA, Rosales TI, Kim HS, Ou Y-H, Toombs JE, et al. Mode of action and pharmacogenomic biomarkers for exceptional responders to didemnin B. Nat Chem Biol. 2015; 11:401–8. [PubMed: 25867045]
21. Kim HS, Mendiratta S, Kim J, Pecot CV, Larsen JE, Zubovych I, et al. Systematic identification of molecular subtype-selective vulnerabilities in non-small-cell lung cancer. Cell. 2013; 155:552–66. [PubMed: 24243015]

22. Singh A, Greninger P, Rhodes D, Koopman L, Violette S, Bardeesy N, et al. A gene expression signature associated with “K-Ras addiction” reveals regulators of EMT and tumor cell survival. Cancer Cell. 2009; 15:489–500. [PubMed: 19477428]

23. Byers LA, Diao L, Wang J, Saintigny P, Girard L, Peyton M, et al. An epithelial-mesenchymal transition gene signature predicts resistance to EGFR and PI3K inhibitors and identifies Axl as a therapeutic target for overcoming EGFR inhibitor resistance. Clin Cancer Res. 2013; 19:279–90. [PubMed: 23091115]

24. Aigner K, Dampier B, Descovich L, Mikula M, Sultan A, Schreiber M, et al. The transcription factor ZEB1 (deltaEF1) promotes tumour cell dedifferentiation by repressing master regulators of epithelial polarity. Oncogene. 2007; 26:6979–88. [PubMed: 17486063]

25. Clark K, Plater L, Peggie M, Cohen P. Use of the pharmacological inhibitor BX795 to study the regulation and physiological roles of TBK1 and IkappaB kinase epsilon: a distinct upstream kinase mediates Ser-172 phosphorylation and activation. J Biol Chem. 2009; 284:14136–46. [PubMed: 19307177]

26. Zhu Z, Aref AR, Cohoon TJ, Barbie TU, Imamura Y, Yang S, et al. Inhibition of KRAS-driven tumorigenicity by interruption of an autocrine cytokine circuit. Cancer Discovery. 2014; 4:452–65. [PubMed: 24444711]

27. Joung SM, Park Z-Y, Rani S, Takeuchi O, Akira S, Lee JY. Akt contributes to activation of the TRIF-dependent signaling pathways of TLRs by interacting with TANK-binding kinase 1. The Journal of Immunology. 2011; 186:499–507. [PubMed: 21106850]

28. Kim J-Y, Welsh EA, Oguz U, Fang B, Bai Y, Kinose F, et al. Dissection of TBK1 signaling via phosphoproteomics in lung cancer cells. Proc Natl Acad Sci USA. 2013; 110:12414–9. [PubMed: 23836654]

29. Jewell, JL., Guan, K-L. Trends Biochem Sci. Elsevier Ltd; 2013. Nutrient signaling to mTOR and cell growth; p. 1-10.

30. Bonnard M, Mirtsos C, Suzuki S, Graham K, Huang J, Ng M, et al. Deficiency of T2K leads to apoptotic liver degeneration and impaired NF-kappaB-dependent gene transcription. The EMBO Journal. 2000; 19:4976–85. [PubMed: 10990461]

31. Bodemann BO, Orvedahl A, Cheng T, Ram RR, Ou Y-H, Formstecher E, et al. RalB and the exocyst mediate the cellular starvation response by direct activation of autophagosome assembly. Cell. 2011; 144:253–67. [PubMed: 21241894]

32. Magnuson B, Ekim B, Fingar DC. Regulation and function of ribosomal protein S6 kinase (S6K) within mTOR signalling networks. Biochem J. 2012; 441:1–21. [PubMed: 22168436]

33. Laplante, M., Sabatini, DM. Cell. Vol. 149. Elsevier Inc; 2012. mTOR Signaling in Growth Control and Disease; p. 274-93.

34. Kim D-H, Sarbassov DD, Ali SM, King JE, Latek RR, Erdjument-Bromage H, et al. mTOR Interacts with Raptor to Form a Nutrient-Sensitive Complex that Signals to the Cell Growth Machinery. Cell. 2002; 110:163–75. [PubMed: 12150925]

35. Shah OJ, Ghosh S, Hunter T. Mitotic regulation of ribosomal S6 kinase 1 involves Ser/Thr, Pro phosphorylation of consensus and non-consensus sites by Cdc2. J Biol Chem. 2003; 278:16433–42. [PubMed: 12586835]

36. Zhang J, Gao Z, Ye J. Phosphorylation and degradation of S6K1 (p70S6K1) in response to persistent JNK1 Activation. Biochim Biophys Acta. 2013; 1832:1980–8. [PubMed: 23816567]

37. Ye X, Weinberg RA. Epithelial-Mesenchymal Plasticity: A Central Regulator of Cancer Progression. Trends Cell Biol. 2015; 25:675–86. [PubMed: 26437589]

38. Lamouille S, Xu J, Derynck R. Molecular mechanisms of epithelial-mesenchymal transition. Nat Rev Mol Cell Biol. 2014; 15:178–96. [PubMed: 24556840]

39. Shaul YD, Freinkman E, Comb WC, Cantor JR, Tam WL, Thiru P, et al. Dihydropyrimidine accumulation is required for the epithelial-mesenchymal transition. Cell. 2014; 158:1094–109. [PubMed: 25171410]

40. Carretero J, Shimamura T, Rikova K, Jackson AL, Wilkerson MD, Borgman CL, et al. Integrative genomic and proteomic analyses identify targets for Lkb1-deficient metastatic lung tumors. Cancer Cell. 2010; 17:547–59. [PubMed: 20541700]

41. Goodwin JM, Svensson RU, Lou HJ, Winslow MM, Turk BE, Shaw RJ. An AMPK-independent signaling pathway downstream of the LKB1 tumor suppressor controls Snail1 and metastatic potential. Molecular Cell. 2014; 55:436–50. [PubMed: 25042806]

42. Potts MB, Kim HS, Fisher KW, Hu Y, Carrasco YP, Bulut GB, et al. Using functional signature ontology (FUSION) to identify mechanisms of action for natural products. Science Signaling. 2013; 6:ra90. [PubMed: 24129700]

43. Cowley GS, Weir BA, Vazquez F, Tamayo P, Scott JA, Rusin S, et al. Parallel genome-scale loss of function screens in 216 cancer cell lines for the identification of context-specific genetic dependencies. Sci Data. 2014; 1:140035. [PubMed: 25984343]

44. Liu S, Cai X, Wu J, Cong Q, Chen X, Li T, et al. Phosphorylation of innate immune adaptor proteins MAVS, STING, and TRIF induces IRF3 activation. Science. 2015; 347:aaa2630. [PubMed: 25636800]

45. Pillai S, Nguyen J, Johnson J, Haura E, Coppola D, Chellappan S. Tank binding kinase 1 is a centrosome-associated kinase necessary for microtubule dynamics and mitosis. Nature Communications. 2015; 6:10072.

46. Hasan M, Gonugunta VK, Dobbs N, Ali A, Palchik G, Calvaruso MA, et al. Chronic innate immune activation of TBK1 suppresses mTORC1 activity and dysregulates cellular metabolism. Proc Natl Acad Sci USA. 2017; 114:746–51. [PubMed: 28069950]

47. Helgason E, Phung QT, Dueber EC. Recent insights into the complexity of Tank-binding kinase 1 signaling networks: the emerging role of cellular localization in the activation and substrate specificity of TBK1. FEBS Lett. 2013; 587:1230–7. [PubMed: 23395801]

48. Wang F, Alain T, Szretter KJ, Stephenson K, Pol JG, Atherton MJ, et al. S6K-STING interaction regulates cytosolic DNA-mediated activation of the transcription factor IRF3. Nat Immunol. 2016; 17:514–22. [PubMed: 27043414]

49. Pilli M, Arko-Mensah J, Ponpuak M, Roberts E, Master S, Mandell MA, et al. TBK-1 promotes autophagy-mediated antimicrobial defense by controlling autophagosome maturation. Immunity. 2012; 37:223–34. [PubMed: 22921120]

50. Ishikawa H, Ma Z, Barber GN. STING regulates intracellular DNA-mediated, type I interferon-dependent innate immunity. Nature. 2009; 461:788–92. [PubMed: 19776740]

51. Goncalves A, Bürckstümmer T, Dixit E, Scheicher R, Górna MW, Karayel E, et al. Functional dissection of the TBK1 molecular network. PLoS ONE. 2011; 6:e23971. [PubMed: 21931631]

52. Skoulidis F, Byers LA, Diao L, Papadimitrakopoulou VA, Tong P, Izzo J, et al. Co-occurring genomic alterations define major subsets of KRAS-mutant lung adenocarcinoma with distinct biology, immune profiles, and therapeutic vulnerabilities. Cancer Discovery. 2015; 5:860–77. [PubMed: 26069186]

53. Li X, Yang M, Yu Z, Tang S, Wang L, Cao X, et al. The tyrosine kinase Src promotes phosphorylation of the kinase TBK1 to facilitate type I interferon production after viral infection. Science Signaling. 2017; 10

54. Biondini M, Duclos G, Meyer-Schaller N, Silberzan P, Camonis J, Parrini M-C. RalB regulates contractility-driven cancer dissemination upon TGFβ stimulation via the RhoGEF GEF-H1. Sci Rep. 2015; 5:11759. [PubMed: 26152517]

55. Liu W, Huang Y-J, Liu C, Yang Y-Y, Liu H, Cui J-G, et al. Inhibition of TBK1 attenuates radiation-induced epithelial-mesenchymal transition of A549 human lung cancer cells via activation of GSK 3β and repression of ZEB1. Lab Invest. 2014; 94:362–70. [PubMed: 24468793]

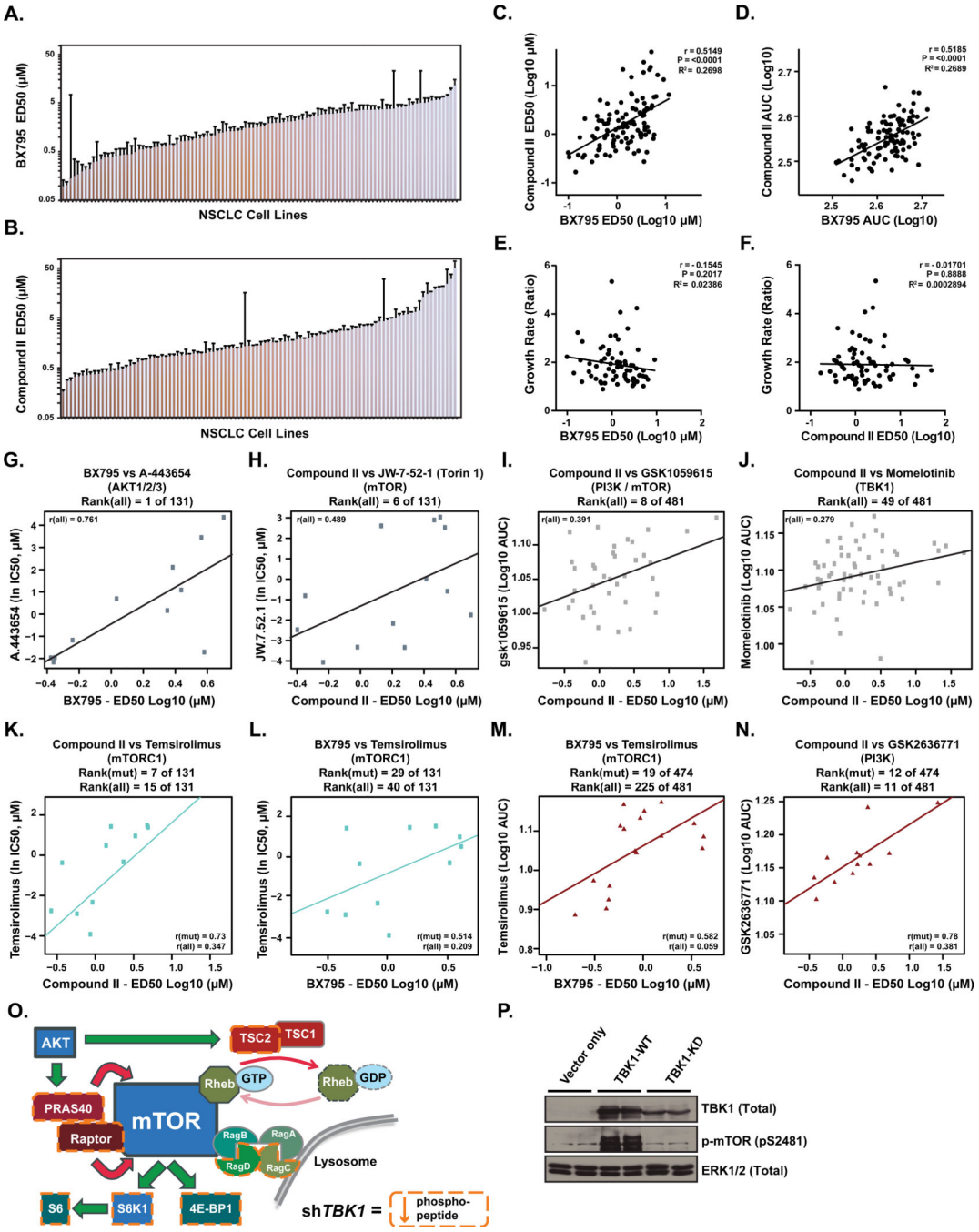

Figure 1. Chemical breadth of efficacy screens in NSCLC lines indicate extensive correlation between TBK1 and AKT/mTOR inhibitor sensitivity

(A–B) Sensitivity profiles of (A) BX795 and (B) Compound II in 100 NSCLC cell lines. Error bars = standard deviation (SD) above the mean ED50 values of the most-concordant replicates (n = 2). See also Table S1 & Materials and Methods.

(C–F) BX795 and Compound II correlate significantly with each other, but not cell growth rates. Correlations of (C) BX795 ED50 (Log_{10}) vs. Compound II ED50 (Log_{10}). (D) BX795 Area-Under-the-Curve (AUC) (Log_{10}) vs. Compound II AUC (Log_{10}). (E) Log_{10} BX795 ED50 or (F) Log_{10} Compound II ED50 vs. cell line growth rates (reported as a ratio of (Day

5:Day1) to (Day3:Day1) growth rate ratios). Inset: Pearson Correlation (r), correlation p-value (P), and goodness of fit (R^2).

(G–N) TBK1 inhibitors correlate consistently with AKT/mTOR Pathway inhibitors from (16) (G–H, K–L) and (17) (I–J, M–N). (G) BX795 vs. A-443654 (AKT1/2/3 inhibitor). (H) Compound II vs. JW-7-52-1 (Torin 1) (mTOR inhibitor). (I) Compound II vs. GSK1059615 (PI3K/mTOR inhibitor). (J) Compound II vs. Momelotinib (CYT387) (JAK/TBK1/IKKe inhibitor). (K) Compound II vs. Temsirolimus (mTORC1 inhibitor). (L–M) BX795 vs. Temsirolimus. (N) Compound II vs. GSK2636771 (PI3K inhibitor). Scatterplots depict correlations calculated among all (G–J) or *KRAS*-mutant only (K–N) NSCLC lines tested. Log10-transformed BX795 or Compound II ED50 sensitivity values are plotted along the x-axes, while published inhibitor sensitivity values from (16) (ln IC50) or (17) (Log10-transformed AUC) are plotted along the y-axes. Also listed are correlation rank and Pearson correlation values among all (r(all)) or *KRAS*-mutant only (r(mut)) NSCLC lines tested. See also Table S2.

(O) shRNA-mediated depletion of *TBK1* in A549 cells exhibits decreased phosphorylation of mTORC1 regulatory elements (summarized from (28)).

(P) Transient overexpression of TBK1 induces mTOR-S2481 phosphorylation in a kinase-dependent manner in HEK293FT cells. WT = Wild type, KD = Kinase Dead (K38M) Mutant.

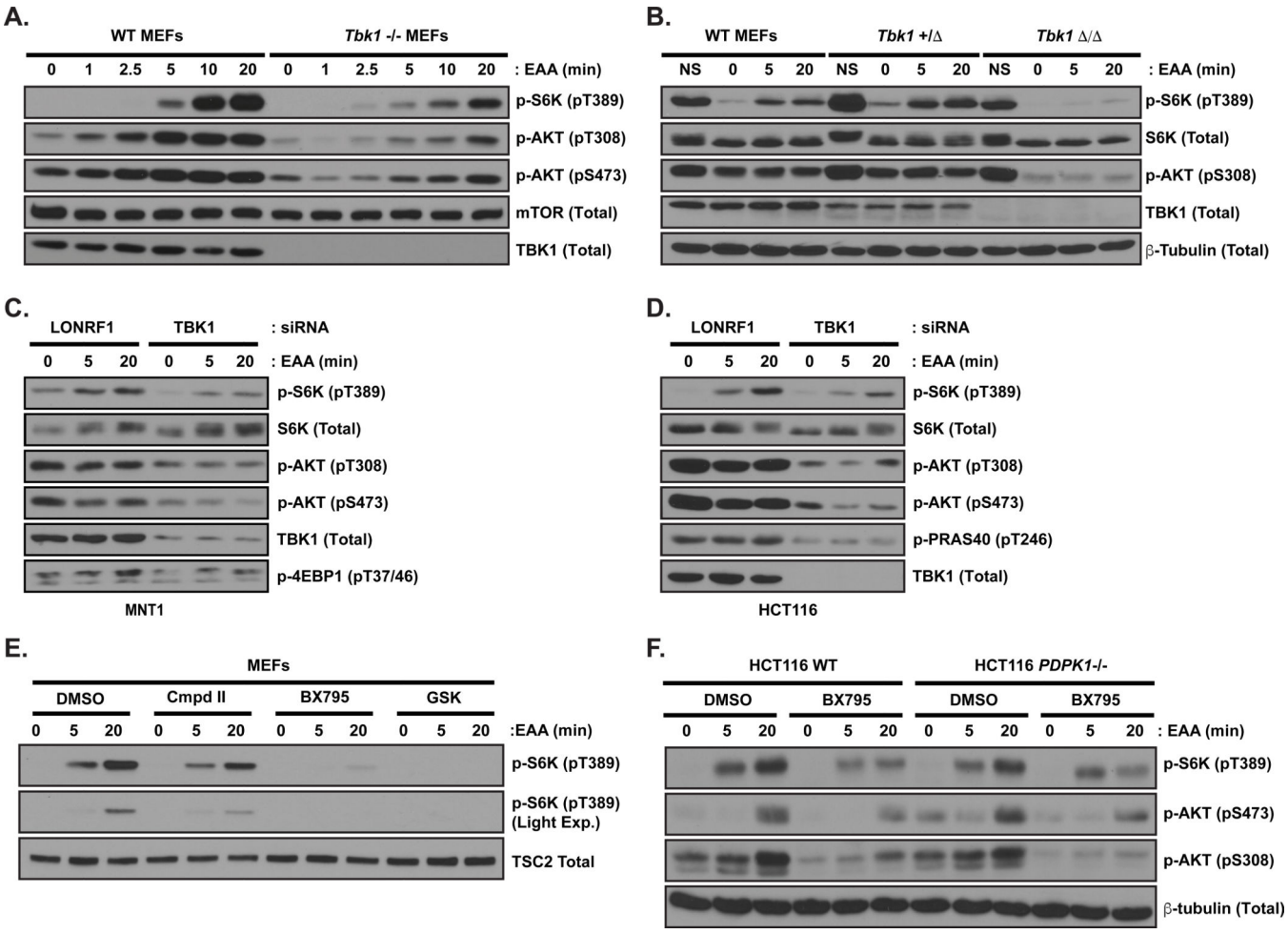

Figure 2. TBK1 supports AKT/mTORC1 activation during an amino acid starved-to-fed state transition

(A) *Tbk1* homozygous knock-out (−/−) Mouse Embryonic Fibroblasts (MEFs) exhibit blunting of essential amino acid (EAA)-dependent AKT/mTORC1 activation, compared to *Tbk1* wild-type (WT) MEFs as readout by activating phosphorylation of AKT (pT308, pS473) and mTORC1 phosphorylation of S6K (pT389). Here and in Figure 2B–F, cells were nutrient starved for 3 hours in EBSS (including priming with 1mM Gln for the final hour of starvation). EAA were then added for the indicated times. See also Materials and Methods.

(B) *Tbk1* homozygous N-terminal truncation mutant (Δ/Δ), but not homozygous wild-type (WT) or heterozygous mutant (+/Δ) MEFs exhibit blunting of EAA-dependent AKT/mTORC1 activation as readout by activating phosphorylation of AKT (pT308), S6K (pT389), and positive feedback phosphorylation on mTOR by S6K (pS2448). NS = no starvation or simulation (cells in culture media only).

(C–D) 72-hr transfection of *TBK1* or *LONRF1* (non-specific control) siRNA pools of three independent oligo duplexes blunts activation of AKT/mTORC1 signaling in cancer cells ((C) MNT1 (melanoma) or (D) HCT116 (colorectal)). Additional readouts for AKT/mTORC1 activity include (C) mTORC1 phosphorylation of 4EBP1 (pT37/46) and (D) AKT phosphorylation of PRAS40 (pT246).

(E) TBK1 inhibitors inhibit mTORC1 activation by EAA in *Trp53*−/− immortalized MEFs. DMSO or 2μM Compound II, BX795 or GSK2292978A (GSK) was added after starvation, 2hr before addition of EAA for the indicated times.

(F) BX795 blunts AKT/mTORC1 activation by EAA in a *PDPK1*-independent manner. *PDPK1* WT or knock-out (−/−) HCT116 cells were treated with DMSO or 0.5μM BX795 after starvation, 30 min before addition of EAA for the indicated times.

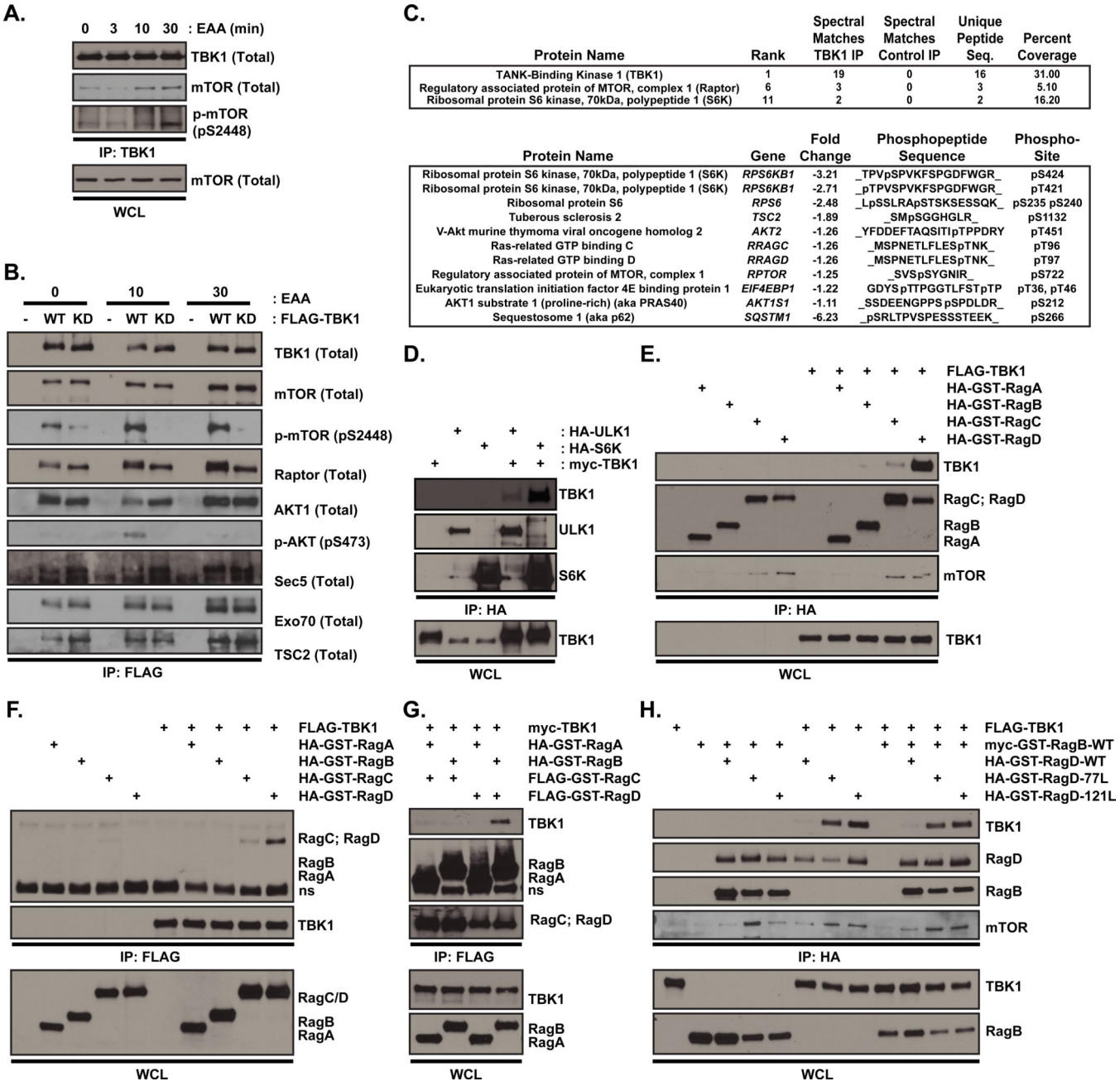

Figure 3. TBK1 is physically associated with multiple AKT/mTOR regulatory elements

(A) EAA stimulation induced the association of mTOR with TBK1 in a time-dependent manner. HEK293T were starved in EBSS for 3 hours (primed with 2mM Gln and 10μM Insulin during the final hour of starvation) and endogenous TBK1 was immunoprecipitated (IP) with an anti-TBK1 antibody before or after the addition of EAA for the indicated times. (B) TBK1 can associate with multiple endogenous AKT/mTORC1 regulatory elements. HEK293T cells were starved in EBSS (w/ 10% FBS) for 50 min, followed by EAA addition for the indicated times prior to immunoprecipitation of ectopically expressed wild type (WT) or kinase-dead (KD, K38M) TBK1 with an anti-FLAG-tag antibody.

(C) Proteomic analysis of TBK1 interactor network space. (Upper) Summary of anti-3XFLAG-TBK1 IP-mass spectrometry I.D.s, including ranking, numbers of spectral matches and unique peptide sequences identified, and percent total protein coverage in TBK1 vs. control (empty vector) IPs. See also Materials and Methods. (Lower) Summary of abundance fold-changes of phospho-peptides corresponding to AKT/mTORC1 regulatory elements, upon shRNA-mediated depletion of *TBK1* in A549 cells (modified from (28), See also Figure 1O).

(D) Selective interaction of TBK1 and S6K. Co-expression of myc-TBK1 and HA-S6K or HA-ULK1 (another mTORC1 substrate) in HEK293T was followed by IP with an anti-HA antibody (IB: anti-TBK1, -ULK1, -S6K).

(E–F) Selective interaction of TBK1 and RagD. Co-expression of FLAG-TBK1 with HA-GST-RagA, -RagB, -RagC, or –RagD in HEK293T was followed by (E) IP with an anti-HA antibody (IB: anti-FLAG, -HA, -mTOR) or (F) IP with an anti-FLAG antibody (IB: anti-FLAG, -HA), ns = non-specific.

(G) Selective interaction of TBK1 with RagB/D heterodimers. Co-overexpression of myc-TBK1 with HA-GST-RagA or -RagB and FLAG-GST-RagC or -RagD in HEK293T was followed by IP with an anti-FLAG antibody (IB: anti-FLAG, -HA, or -TBK1), ns = non-specific.

(H) The RagD/TBK1 interaction is independent of RagD GDP/GTP status. Co-expression of FLAG-TBK1 and myc-GST-RagB-WT with HA-GST-RagD-WT, -RagD-77L (GDP-bound mutant), or -RagD-121L (GTP-bound mutant) in HEK293T was followed by IP with an anti-HA antibody (IB: anti-FLAG, -HA, -myc, -mTOR).

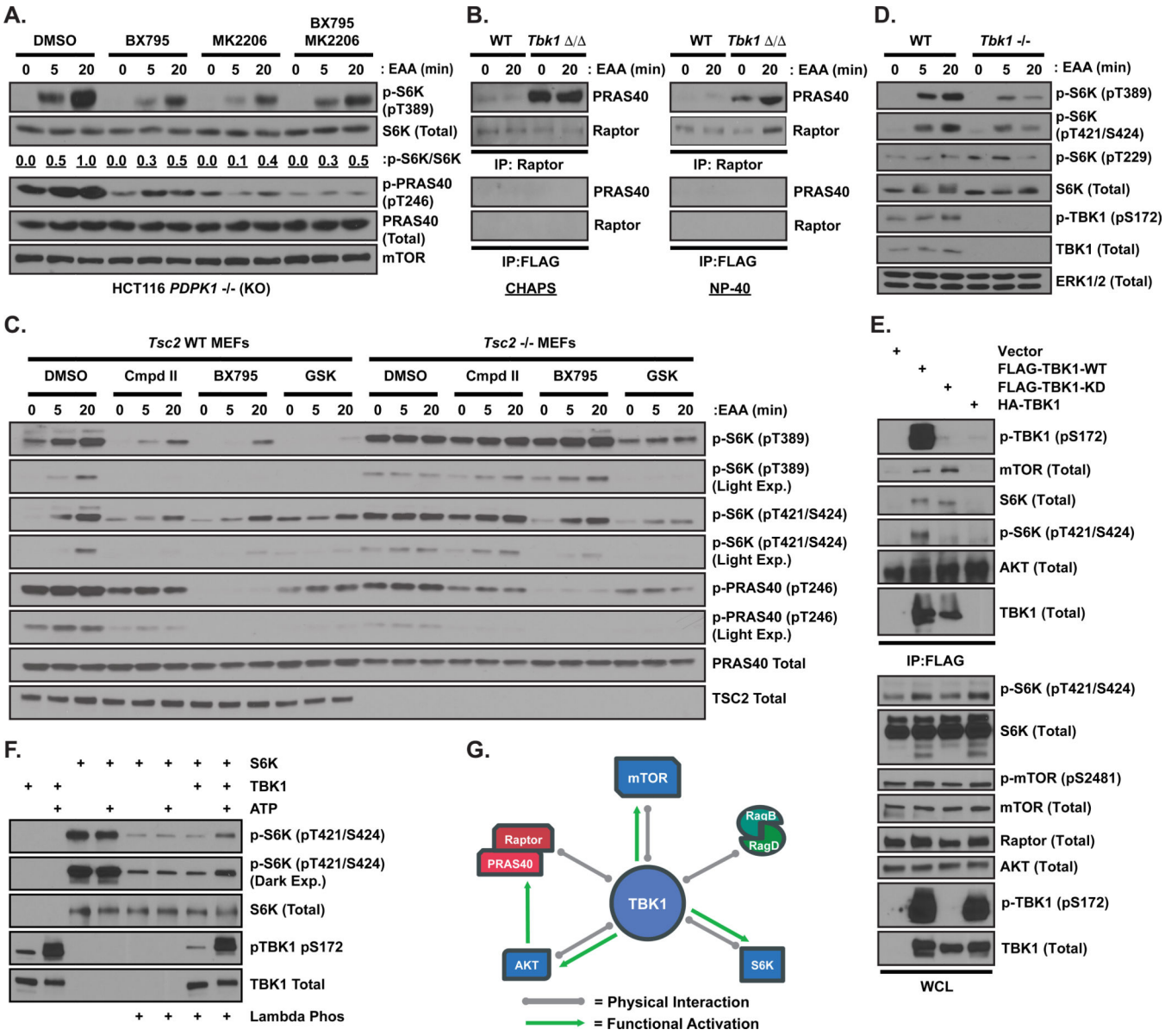

Figure 4. TBK1 supports mTORC1 pathway activation both upstream and downstream of mTOR

(A) Inhibition of TBK1 or AKT similarly blunts mTORC1 activation alone or together in *PDPK1*-null (−/−) HCT116 cells. Cells were starved in EBSS for 3 hrs in the presence of DMSO or 0.5μM MK2206 (allosteric AKT inhibitor). Following starvation, but prior to EAA addition at the indicated times, cells were treated with DMSO or 0.5μM BX795 in EBSS for 30 min. mTORC1 phosphorylation of S6K (pT389) and AKT phosphorylation of PRAS40 (pT246) were assessed via immunoblot. Densitometry ratios for S6K (pT389)/S6K (Total) were calculated via ImageJ and are listed relative to the 20 min EAA time point in the DMSO-treated condition.

(B) TBK1 loss of function corresponds to increased PRAS40-mTORC1 association. Endogenous Raptor was immunoprecipitated from *Tbk1* WT or (Δ/Δ) MEFs. Elevated

affinity of PRAS40 for Raptor in (Δ/Δ) MEFs was maintained under (Left) 0.3% CHAPS or (Right) 0.5% NP-40 cell lysis conditions. Control = IP with an anti-FLAG-tag antibody.

(C) TBK1 inhibitors partially blunt AKT/mTORC1 signaling in *Tsc2* WT or homozygous knock-out (−/−) *Trp53* −/− immortalized MEFs. DMSO or 2μM Compound II, BX795 or GSK2292978A (GSK) was added after starvation, 30 min before addition of EAA for the indicated times.

(D) TBK1 is required for an amino acid-induced S6K C-terminal autoinhibitory domain phosphorylation at pT421/S424. Loss of TBK1 also attenuated TBK1 autophosphorylation (pS172) and the activating phosphorylation of S6K by mTORC1 (pT389), but not PDK1 (pT229) upon EAA stimulation in *Tbk1* −/− MEFs

(E) S6K is phosphorylated in its autoinhibitory domain in a TBK1 kinase-dependent manner in TBK1 complexes. Myc-vector-only, myc-FLAG-TBK1-WT, myc-FLAG-TBK1-KD, or HA-TBK1 were overexpressed in HEK293FT cells, followed by anti-FLAG IP. WCL = whole cell lysate.

(F) TBK1 can phosphorylate the autoinhibitory domain of S6K *in vitro*. Recombinant TBK1 and S6K (pretreated with lambda phosphatase) were incubated either alone or together in the presence or absence of 200μM ATP. ATP-dependent phosphorylation of TBK1 and S6K were assessed by immunoblot as indicated.

(G) TBK1 physically and functionally interacts with multiple AKT/mTORC1 regulatory elements. In this cartoon, green arrows point toward nodes whose activity is directly or indirectly promoted by TBK1, whereas grey lines indicate points of physical association with TBK1.

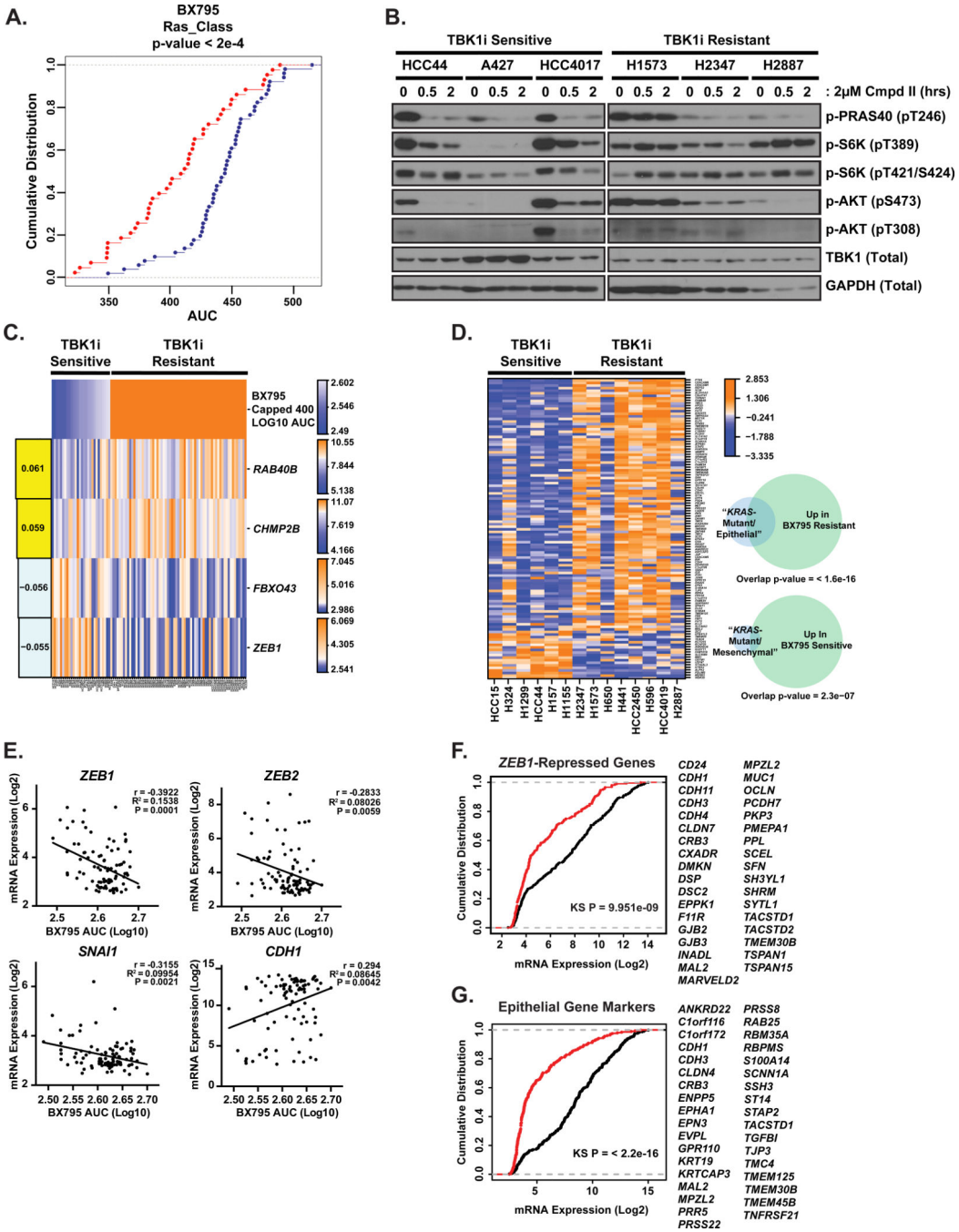

Figure 5. Identification of a TBK1-dependent Molecular Subtype of NSCLC Cells

(A) "Ras-Class"-mutant NSCLC cell lines are preferentially sensitive to TBK1 inhibition (TBK1i). A Cumulative Distribution Function (CDF) plot comparing BX795 AUC of cell lines with "Ras-Class" mutations (*KRAS, NRAS, HRAS, PIK3CA*, or *BRAF*) (red) (n=43) vs. "Ras-Class" wild-type cell lines (blue) (n = 51). Kolmogorov–Smirnov (KS)-test p-value = < 2e– 04. See also Materials and Methods.

(B) Steady-state AKT/mTORC1 signaling was selectively attenuated by Compound II in TBK1i-senstive but not TBK1i-resistant/*KRAS*-mutant NSCLC. 2μM Compound II was

added to the culture media of *KRAS*-Mutant NSCLC cell lines (HCC44, A427, HCC4017, H1573, H2347, H2887) for 0.5 or 2 hours.

(C) Elastic net modeling returned a quantitative 4-gene expression signature predicting sensitivity to BX795. AUC (values capped at 400) is indicated as a heatmap in the top panel with gene expression (log_2) plotted underneath. A key to interpret the color scale is plotted to the right and elastic net-derived weights are plotted as a bar graph to the left. Source data: GEO: GSE32036.

(D) "Ras-Class"-mutant/TBK1i-sensitve NSCLC cell lines have mesenchymal gene expression features. Heatmap indicating top 5% most differentially expressed mRNAs between "Ras-Class"-mutant/TBK1i-sensitive versus -resistant cell lines, plotted as z-scores for expression. Venn diagrams represent overlap between genes upregulated in the indicated classes and the *KRAS*-mutant/mesenchymal ($p<1.6E-16$) and *KRAS*-mutant/epithelial ($p=2.3E-7$) gene signatures (22). Source data: GEO: GSE32036.

(E) Scatterplots of BX795 AUC (Log_{10}) sensitivity values vs. mRNA expression (Log_2) of EMT Markers (*ZEB1, ZEB2, SNAI1, CDH1*) in the NSCLC cell line panel. Inset: Pearson Correlation (r), correlation p-value (P), and goodness of fit (R^2). See also Table S3. Source data: GEO: GSE32036.

(F–G) CDF plots for mRNA expression (Log_2) of (F) *ZEB1*-repressed epithelial genes (24) (KS-test p-value = 9.951e-09) or (G) epithelial state gene markers (23) (KS test P value = < 2.2e-16) in "Ras-Class"-mutant/TBK1i-sensitive (red) vs. "Ras-Class"-mutant/TBK1i-resistant (black) NSCLC cell lines used in Figures 5D and S3D–E. Source data: GEO: GSE32036.

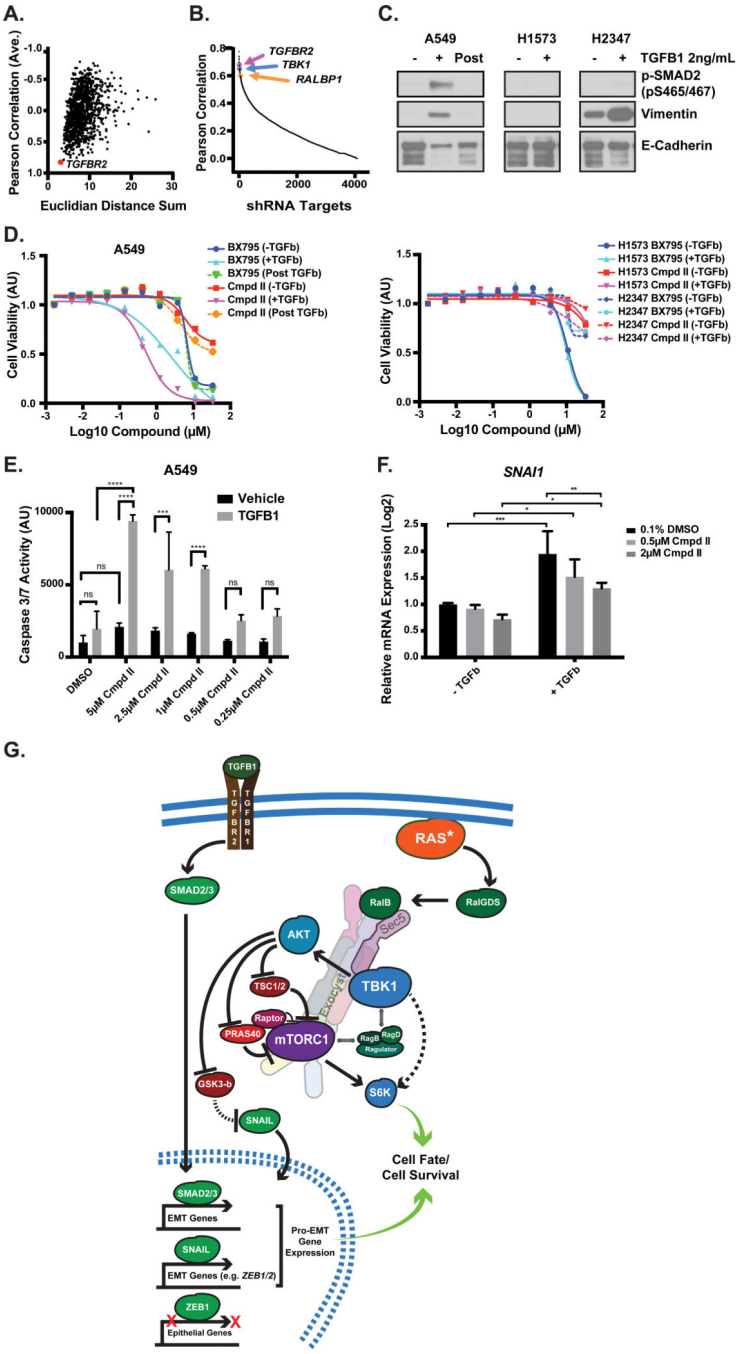

Figure 6. Modulation of Mesenchymal Status is Sufficient to Alter Ras-Mutant NSCLC Sensitivity to TBK1 Inhibitors

(A–B) Guilt-by-association relationship between TBK1 and Transforming Growth Factor-Beta Receptor 2 (TGFBR2) signaling in cancer cells. (A) Scatterplot of siRNAs and miRNAs within FUSION as a function of their unsupervised hierarchical cluster distances from si*TBK1* (as a function of average Pearson correlation or Euclidian distance sum) (42). (B) Toxicity profile correlations between BX795 ED50 and >4000 shRNAs in NSCLC cell lines (43), ranked by Pearson correlation (> 0). Arrows indicate shRNAs against *TGFBR2, TBK1*, and RalA/B effector, *RALBP1.*

(C–D) *KRAS*-mutant NSCLC cells undergoing TGF-beta-mediated EMT are sensitized to TBK1 inhibitors. Culture of A549, but not H1573 or H2347, cells in TGF-beta (2ng/mL)-conditioned media induced mesenchymal protein expression (C) and increased sensitivity to TBK1i (D). Re-culture of TGF-beta-adapted A549 cells in normal media reversed EMT features (C) and TBK1i sensitization (D). Cells were cultured either in normal media (-TGFb), in media supplemented with 2ng/mL TGF-beta (+ TGFb), or in TGF-beta-free media after TGF-beta adaptation (Post TGFb). Data from the 3 cell lines in (C) are derived from the same immunoblots, however extraneous lanes between A549 and H1573, and between H1573 and H2347, have been cropped out to aid in reading the results.

(E) Compound II synergizes with short-term TGF-beta treatment to enhance apoptosis in A549. Apoptosis induction was readout by caspase 3/7 activity via the Caspase Glo Assay. Cells were treated with 10ng/mL TGF-beta for 24 hrs followed by 24 hr treatment with DMSO or Compound II as listed. Error bars = standard deviation from the mean. Statistical significance was calculated using One-Way ANOVA, with Tukey's multiple comparisons test, *** = $P < 0.001$, **** = $P < 0.0001$, ns = not significant.

(F) TBK1 supports TGF-beta-induced induction of EMT early response gene (*SNAI1*) expression. A549 cells were treated with DMSO or Compound II as listed for 30 min followed by addition of 10ng/mL TGF-beta for 24 hrs. mRNA expression is reported in Log_2 values normalized to *GAPDH* (data not shown). Error bars = standard deviation from the mean. Statistical significance was calculated as in 6E, *$P < 0.05$, **$P < 0.01$, ***$P < 0.001$

(G) Model whereby TBK1 supports pro-survival/cell fate signaling downstream of Ras and EMT/TGF-beta signaling through newly characterized regulation of AKT/mTORC1 signaling.